



Published in final edited form as:

Bioorg Med Chem. 2008 April 1; 16(7): 3848–3865. doi:10.1016/j.bmc.2008.01.044.

Constrained NBMPR Analogue Synthesis, Pharmacophore Mapping and 3D-QSAR Modeling of Equilibrative nucleoside Transporter 1 (ENT1) Inhibitory Activity

Zhengxiang Zhu and John K. Buolamwini*

Department of Pharmaceutical Sciences, College of Pharmacy, University of Tennessee Health Science Center, Memphis, TN 38163

Abstract

Conformationally constrained analogue synthesis was undertaken to aid in pharmacophore mapping and 3D QSAR analysis of nitrobenzylmercaptapurine riboside (NBMPR) congeners as equilibrative nucleoside transporter 1 (ENT1) inhibitors. In our previous study (Zhu *et al.*, *J. Med. Chem.* 46, 831–837, 2003), novel regioisomeric nitro-1, 2, 3, 4-tetrahydroisoquinoline conformationally constrained analogues of NBMPR were synthesized and evaluated as ENT1 ligands. 7-NO₂-1, 2, 3, 4-tetrahydroisoquino-2-yl purine riboside was identified as the analogue with the nitro group in the best orientation at the NBMPR binding site of ENT1. In the present study, further conformational constraining was introduced by synthesizing 5'-O, 8-cyclo derivatives. The flow cytometrically determined binding affinities indicated that the additional 5'-O, 8-cyclo constraining was unfavorable for binding to the ENT1 transporter. The structure-activity relationship (SAR) acquired was applied to pharmacophore mapping using the PHASE program. The best pharmacophore hypothesis obtained embodied an *anti*-conformation with three H-bond acceptors, one hydrophobic center, and two aromatic rings involving the 3'-OH, 4'-oxygen, the NO₂ group, the benzyl phenyl and the imidazole and pyrimidine portions of the purine ring, respectively. A PHASE 3D-QSAR model derived with this pharmacophore yielded an r^2 of 0.916 for four (4) PLS components, and an excellent external test set predictive r^2 of 0.78 for 39 compounds. This pharmacophore was used for molecular alignment in a comparative molecular field analysis (CoMFA) 3D-QSAR study that also afforded a predictive model with external test set validation predictive r^2 of 0.73. Thus, although limited, this study suggests that the bioactive conformation for NBMPR at the ENT1 transporter could be *anti*. The study has also suggested an ENT1 inhibitory pharmacophore, and established a predictive CoMFA 3D-QSAR model that might be useful for novel ENT1 inhibitor discovery and optimization.

Introduction

Nucleoside transport inhibitors (NTIs) have been shown to have potential therapeutic applications in heart disease,^{2,3,4,5,6} inflammatory disease,⁷ viral infections,^{8,9} and cancer chemotherapy.^{10,11,12,13,14,15} The ENT1 transporter, which is the focus of this research, is the major nucleoside transporter in most mammalian tissues, especially heart tissue,^{16,17} and appears to be the most relevant NT target for therapeutic exploitation. Several chemical classes

*Author to whom correspondence should be addressed at: Department Pharmaceutical Sciences, College of Pharmacy, University of Tennessee Health Science Center, 847 Monroe Avenue, Suite 327, Memphis, TN 38163, Phone: (901) 448-7533, Fax: (901) 448-6828, jbuolamwini@utm.edu.

Publisher's Disclaimer: This is a PDF file of an unedited manuscript that has been accepted for publication. As a service to our customers we are providing this early version of the manuscript. The manuscript will undergo copyediting, typesetting, and review of the resulting proof before it is published in its final citable form. Please note that during the production process errors may be discovered which could affect the content, and all legal disclaimers that apply to the journal pertain.

have been shown to inhibit the ENT1,¹⁸ the most potent and selective of which are NBMMPR and its congeners, which inhibit it at low nanomolar to subnanomolar concentrations.¹⁹ Unfortunately, attempts at therapeutic application of current ENT1 inhibitors have been largely disappointing due to their poor pharmacological profiles with regard to toxicity, selectivity, and poor *in vivo* efficacy.¹⁸ Thus, there is a need for novel inhibitors.

Since there are no 3D structures of mammalian nucleoside transporters nor their complexes with inhibitors, knowledge of the 3D pharmacophore of the most potent and selective inhibitors will be useful for rational design of new NT inhibitors.²⁰ To that end, the objective of this study was to continue our probe the bioactive conformation of NBMMPR and its analogues as ENT1 nucleoside transporter inhibitors through a combination of conformationally constrained analogues synthesis¹, pharmacophore mapping, and 3D-QSAR modeling. Current structure-activity relationship (SAR) studies on ENT1 nucleoside transport inhibitors¹⁸ demonstrate that for NBMMPR analogues, the nitrobenzyl moiety is critical for high affinity binding to the transporter. Therefore, in our previous study, a series of conformationally constrained analogues of NBMMPR was synthesized by replacing the purine 6-position nitrobenzyl group with nitro-1, 2, 3, 4-tetrahydroisoquinolines, thereby locking two of the rotatable bonds in the flexible nitrobenzyl moiety into a tetrahydroisoquinoline ring. The most suitable substitution position of the nitro group was explored by varying its position on the aromatic ring of the tetrahydroisoquinoline moiety, as shown in compounds **2–5** (see Figure 1). The results indicated that compound **4** with the nitro substituent at the 7-position of tetrahydroisoquinoline ring most captures the bioactive orientation of the nitrobenzyl moiety of NBMMPR.¹ However, compounds **2–5**, are still flexible; there are three major rotatable bonds, the *N*⁹-*C*^{1'} glycosidic bond, the *C*⁶-*N*⁶ bond, and the *C*^{4'}-*C*^{5'} bond in the molecules. For NBMMPR analogues and other nucleosides, the base moiety can adopt two main orientations relative to the sugar moiety about the *N*⁹-*C*^{1'} glycosidic bond, termed *syn* and *anti*.²¹ In the *syn* orientation, the bulky portion of the base, such as the pyrimidino ring in purine nucleosides or *O*² in pyrimidine nucleosides, is orientated over the sugar ring; and in the *anti*-conformation it is oriented away from the sugar ring. The intermediate conformations between *syn* and *anti* are referred to as *high-anti* and *high-syn*, respectively (see Figure 2). These different conformations might greatly influence the binding affinities of the molecules at the transporter. In continuation of our probing of the bioactive conformation of NBMMPR in this study, another series of further conformationally constrained analogues. In this series, the free rotation of the glycosidic bond was blocked by forming an *O*^{5'}-*C*⁸ linkage. In doing so, the rotation about the *C*^{4'}-*C*^{5'} bond was also blocked. The most suitable position of the nitro group was again explored by varying its position on the aromatic ring of the tetrahydroisoquinoline moiety, as shown in Figure 1 (compounds **6–9**), where the nitro substituent is in the 5-, 6-, 7-, or 8-position of the 1, 2, 3, 4-tetrahydroisoquinoline ring, respectively. The most active NBMMPR analogues including the conformationally constrained analogue, compound **4**, were used to develop a common pharmacophore hypothesis using the PHASE program (Schrödinger), which was subsequently used for CoMFA 3D-QSAR modeling in attempts to validate the suggested conformation.

Chemistry

A limited number of studies have reported the intramolecular cyclization of purine nucleosides. Ikehara *et al.* once reported that by activating the 5'-OH group with sodium hydride in dioxane, the resulting nucleophilic O^- species would attack the electron-deficient carbon at position 8 of 8-bromo-2', 3'-*O*-isopropylideneadenosine to give 5'-*O*, 8-cyclo-2', 3'-*O*-isopropylideneadenosine.²² However, when we tried to follow this method to prepare compound **12** (see Scheme 1), we found we could not obtain compound **11** by bromination of compound **10** (which was prepared from compound **4**) using bromine in the mixture of dioxane and 10% Na_2HPO_4 (1:1) or bromine water in NaOAc buffer as reported in the literature for the synthesis of 8-bromo-2', 3'-*O*-isopropylideneadenosine.^{23,24,25} Instead, the product was identified to be

compound **13** when bromine in dioxane/ Na_2HPO_4 (1:1) was used. No products were obtained when bromine water in NaOAc buffer was used. An alternative strategy employing direct oxidative cyclization of compound **10** to yield **12**, using lead tetraacetate in dry benzene or *N*-halosuccinimide in acetic acid as shown in Scheme 2, which has been previously used to synthesize 5'-*O*, 8-cycloadenosines²⁶ and 5'-*O*, 8-cycloguanosines²⁷, also failed. This led to the conclusion that the nitrotetrahydroisoquinoline substituent at the purine C⁶-position was hindering the 5'-*O*, C-8-cyclization. Therefore, some other reaction schemes with an appropriate substrate other than compound **4** were considered. As shown in Scheme 3, 6-chloropurine riboside (**14**), which does not have a bulky substituent at the 6-position and is commercially available, was chosen. 2', 3'-*O*-isopropylidene-6-chloropurine riboside (**15**) was prepared by treating compound **14** with acetone in the presence of a catalytic amount of hydroperchloric acid (70%). 5'-*O*, 8-cyclo-2', 3'-*O*-isopropylidene-6-chloropurine riboside (**16**) was successfully prepared by treating compound **15** with *N*-iodosuccinimide (NIS) in acetic acid. Unfortunately, the deprotection of the 2', 3'-hydroxyl groups in compound **16** became another problem. When compound **16** was treated with 0.5 N H_2SO_4 at 55 °C for deprotection, a complicated mixture of products was obtained, with the major product being compound **18** instead of the desired compound **17**. No reaction occurred when the temperature was lowered, which led to our trying several other deprotecting reagents such as 80 % CH_3COOH and 80 % CF_3COOH , but none was able to selectively remove the isopropylidene group without cleaving the newly formed 5'-*O*, C-8-cyclo bond in compound **16**. Therefore, other protecting groups that can be removed under milder conditions were sought, and *p*-anisaldehyde was considered. The final synthetic methods are shown in Scheme 4, whereby the 2', 3'-hydroxyl groups of compound **14** were protected with *p*-anisaldehyde catalyzed by zinc chloride to afford compound **19**, which was then subjected to intramolecular cyclization in the presence of NIS in acetic acid at ambient temperature to obtain compound **20**. The 2', 3'-*O*-*p*-anisylidene group in compound **20** was selectively removed in 80 % trifluoroacetic acid at 0 °C to give the desired compound **17** with the 5'-*O*, 8-cyclo bond intact. Coupling of compound **17** with compounds **21–24** in the presence of calcium chloride in refluxing ethanol afforded the target products compounds **6–9**, respectively, according to methods reported in our previous study.¹ The compounds were then tested as ligands of the ENT1 transporter by our reported flow cytometric method.^{1,30,31}

Pharmacophore Mapping and 3D QSAR Studies

Materials and Methods

Data Sets—Three highly potent and selective ENT1 nucleoside transporter inhibitors, NBMPR, compounds **4**, and **25** (see Figure 3), were chosen as the active compound set for generating common pharmacophore hypotheses using the PHASE 1.0 program (Schrödinger Inc. San Diego, CA). The training set used for developing 3D-QSAR models included 77 compounds and comprised a series of compounds with a high diversity in structure and a wide range of ENT1 inhibitory potencies as reported by Paul *et al.*,²⁸ a series of tetrahydroisoquinoline conformationally constrained ENT1 inhibitors reported by us,¹ and a series of 5'-*O*, 8-cyclo conformationally constrained ENT1 inhibitors, reported in this study (see Table 1). The test set included 39 compounds with biological data taken from the literature.^{29,30,31} All the biological data were normalized to the flow cytometrically-determined data for comparison using NBMPR as the standard since it was evaluated by both methods.

Molecular Modeling

Three-dimensional structure building, pharmacophore mapping and CoMFA 3D-QSAR studies were carried out on a Silicon Graphics Octane (R12000) workstation with the IRIX 6.5 operating system running the SYBYL program package, version 7.2 (Tripos Associates, St. Louis, MO) and the PHASE 1.0 program (Shrodinger Inc., San Diego). Molecular energy

minimizations were performed using the Tripos force field with a distance-dependent dielectric constant and the Powell conjugate gradient algorithm with an energy change convergence criterion of 0.001 kcal/mol Å. Partial atomic charges were calculated using the Gasteiger-Huckel program in SYBYL. All the molecules in the present study were aligned to the best-generated pharmacophore hypothesis (Pharm_A) obtained from the PHASE pharmacophore mapping exercise.

Generation of Pharmacophore Models

PHASE 1.0 implemented in the Maestro 7.0 modeling package (Schrödinger Inc. San Diego, CA) was used to generate pharmacophore models for ENT1 inhibitors. The 3D structures of all the molecules used in PHASE were built in, and imported from SYBYL. Conformers of each molecule were generated using the MMFFs forcefield in the PHASE program. Pharmacophore feature sites for the molecules were assigned using a set of features defined in PHASE as: hydrogen bond acceptor (A), hydrogen bond donor (D), hydrophobic group (H), negatively charged group (N), positively charged group (P), and aromatic ring (R). Three highly active compounds, NBMPR, compounds **4**, and **25** were selected for generating the pharmacophore hypotheses (see Figure 3). Common pharmacophore hypotheses were identified using conformational analysis and a tree-based partitioning technique. The resulting pharmacophores were then scored and ranked. Pharmacophores with high-ranking scores were validated by a partial least square (PLS) regression-based PHASE 3D-QSAR cross validation, and the best pharmacophore hypothesis identified was further validated by CoMFA 3D-QSAR modeling. All the molecules used for QSAR studies were aligned to the pharmacophore hypothesis obtained in PHASE (see Figure 5).

Development of a CoMFA 3D QSAR Model

The PHASE-generated 3D pharmacophore was used as the alignment template for the CoMFA 3D-QSAR model. CoMFA descriptors were calculated using a sp^3 hybridized carbon probe atom with a van der Waals radius of 1.52 Å and a charge of +1.0 on a 2 or 1 Å spaced 3D cubic lattice with an extension of 4 Å units in all directions to encompass the aligned molecules. Steric (Lennard-Jones 6–12 potential) field energies and electrostatic (Coulombic potential) fields at each lattice point were generated and scaled by the CoMFA-STD method in SYBYL. The SYBYL default energy cut-off of 30 kcal/mol was used to ensure that there would be no extreme energy terms to distort the CoMFA models.

In deriving CoMFA 3D-QSAR models PLS regression analysis was used to correlate the CoMFA descriptors with biological activities. The CoMFA descriptors were used as independent variables, and biological activities (pIC_{50} values) were used as dependent variables. The predictive value of the models was evaluated first by leave-one-out (LOO) cross-validation. The cross-validated coefficient, q^2 , was calculated using Eq.1 as follows:

$$q^2 = 1 - \frac{\sum(Y_{\text{predicted}} - Y_{\text{observed}})^2}{\sum(Y_{\text{observed}} - Y_{\text{mean}})^2}. \quad \text{Eq. 1}$$

where $Y_{\text{predicted}}$, Y_{observed} , and Y_{mean} are the predicted, observed, and mean values of the target property (pIC_{50}), respectively. $\sum(Y_{\text{predicted}} - Y_{\text{observed}})^2$ is the predictive error sum of squares (PRESS). The number of components corresponding to the lowest PRESS value was selected for deriving the final PLS regression models to minimize the tendency to overfit the data. In addition to the q^2 , the number of components, the conventional correlation coefficient r^2 and its standard error s were also computed. CoMFA coefficient maps were generated by interpolation of the pair-wise products between the PLS coefficients and the standard

deviations of the corresponding CoMFA descriptor values. Robustness of the CoMFA models was checked by group cross validation and randomization of activity values (Table 8).

Results and Discussion

ENT1 inhibitory activity of novel 5'-O, 8-linkage constrained nitrotetrahydroisoquinoline NBMPR analogues

The solid-state conformation of NBMPR has been determined by X-ray diffraction,³² and a solution conformation has been proposed using NMR.³³ The X-ray structure reveals the preponderance of a *syn* orientation of the purine ring relative to the sugar moiety, whereas the NMR structure reveals a *high-anti* orientation. However, the orientation about the glycosidic bond in the bioactive conformation remains unknown. The objective of this study was to probe the bioactive orientation of the purine ring relative to the sugar moiety about the glycosidic linkage in NBMPR and its analogues when bound to the ENT1 nucleoside transporter.

The new constrained analogues of NBMPR, compounds **6–9**, in which the 5'-O, 8-linkage blocks the rotation about both the glycosidic bond and C^{4'}-C^{5'} bond, were synthesized as detailed in the chemistry section and evaluated as ENT1 transporter ligands by a flow cytometric binding assay using the K562 chronic myelogenous leukemia cell line as previously described.¹ The concentration-dependent inhibitory curves are depicted in Figure 4 and K_i values are presented in Table 3. These analogues exhibited a broad range of binding affinities at the ENT1 nucleoside transporter. Three of them, compounds **6**, **7** and **9** exhibited low binding affinities, with K_i values in the micromolar range, whereas compound **8**, the cyclonucleoside analogue corresponding to compound **4**, the most tightly bound compound of the previous tetrahydroisoquinoline series¹, bound tightly to the transporter with a nanomolar K_i value of approximately 19 nM. The differences emphasize the remarkable regioselectivity of ENT1 among these tetrahydroisoquinoline NBMPR analogues with respect to the NO₂ substituent.^{28,34} Compared to their less constrained counterparts compounds **2–5**, the binding affinities of compounds **6–9** were significantly lower (see Table 4, K_i values increased from the nanomolar range to the micromolar range except for compound **8**). These results are interesting since compounds **6–9** were obtained by just forming a 5'-O, 8-linkage to block the free rotation of the N⁹-C^{1'} glycosidic bond in compounds **2–5**, respectively. The significant loss in binding affinities in going from compounds **2–5** to compounds **6–9** indicates that not only is the NBMPR binding site regioselective with respect to the nitro substituent, but it is also very sensitive to the orientation of the purine ring about the glycosidic linkage. The 5'-O, 8-cyclo analogues appear not to present a favorable conformation for binding to ENT1, supposing other factors are not in play. However, the fact that compound **8** still exhibited good binding affinity at the transporter implies that the conformation of compound **8** does not deviate too far from the binding mode of NBMPR. These results shed more light on the bioactive conformation of NBMPR. On the other hand, it might be that moving C^{5'} and O^{5'} up to join with C⁸ creates unfavorable interactions at the transporter that were absent in the non-cyclo compounds **2–5**, where the O^{5'} is in a free hydroxyl group (5'-OH) which could participate in both H-bond donor and acceptor interactions. Previous studies, however, suggest that H-bond interactions do not appear to be critical at the 5'-position,^{29, 35} and thus it might be the loss of flexibility (lower entropy) imposed by cyclization that accounts for the low activity.

We continued to carry out pharmacophore mapping and 3D QSAR studies to explore the possible bioactive conformation(s). Pharmacophore modeling is used to propose the 3D spatial arrangement of chemical features that are essential for biological activity of molecules with respect to a biological target. Three-dimensional quantitative structure-activity relationship (3D QSAR) techniques such as comparative molecular field analysis (CoMFA),³⁶ have been successfully applied in many aspects regarding drug design and discovery.³⁷ The CoMFA technique uses both statistical techniques and molecular graphics to determine correlations

between structural properties of molecules and their biological activity. The bioactive conformation of each molecule is chosen and superimposed in a manner supposed to be the interacting mode with the target receptor. The steric and electrostatic fields around the molecules are then correlated with biological activity. The potent ENT1 inhibitors, NBMMPR, compound **4**, and compound **25** (see Figure 3) were used for pharmacophore generation with the PHASE program (Schrodinger). The inclusion of compound **4**, which is a very potent constrained analogue of NBMMPR, markedly reduced the conformational space that the program had to sample, thereby cutting down on analysis time and reducing the number of potential pharmacophore hypothesis to be evaluated. This is a significant advantage over using only flexible NBMMPR analogues. The top five ranking pharmacophore hypotheses generated were validated by PHASE 3D-QSAR analysis involving a test set validation. The resulting best pharmacophore model from that analysis was further validated by CoMFA 3D-QSAR modeling.

For CoMFA 3D-QSAR modeling, an alignment rule for superposition of the 3D structures of the molecules in a “bioactive” conformation is required. In the absence of a crystal structure of the target or a complex of target and ligands, a pharmacophore-based alignment rule is the accepted norm. Thus we employed the PHASE pharmacophore hypothesis generation and validation to obtain an alignment template for the compounds. All the features defined in PHASE: hydrogen bond acceptor (A), hydrogen bond donor (D), hydrophobic group (H), negatively charged group (N), positively charged group (P), and an aromatic ring (A) were considered for the pharmacophore generation. All the novel conformationally constrained analogues of NBMMPR synthesized in our previous study¹ and this study, were included in the training set. All the 77 compounds shown in Table 1 were used to develop the PHASE 3D-QSAR models. All the 39 compounds in Table 2 were used as an external test set for PHASE 3D-QSAR model validations for predictive ability. The top five ranking pharmacophore hypotheses and their feature compositions are shown in Table 5. The PLS results of the five PHASE 3D-QSAR models developed from them and the corresponding prediction results of test set data are listed in Table 6.

All the top five pharmacophore models comprised six features (see Table 5). Pharm_A, Pharm_B and Pharm_D consisted of three hydrogen bond acceptors, one hydrophobic group, and two aromatic rings. Pharm_C and Pharm_E are composed of two hydrogen bond acceptors, one hydrogen bond donor, one hydrophobic group and two aromatic rings. All the five top pharmacophores considered had an *anti*-conformation. These pharmacophore hypotheses afforded PHASE 3D-QSAR models with good PLS statistics results (especially with regard to conventional r^2). However, only one of them, Pharm_A, performed excellently on prediction of the external test set (see Table 6). The Pharm_A pharmacophore produced a PHASE 3D-QSAR model with r^2 of 0.916, four (4) PLS components, and an excellent external test set predictive r^2 of 0.777. The large value of F indicates a statistically significant regression model, which is supported by the small value of the variance ratio (P), an indication of a high degree of confidence (PHASE user manual). This pharmacophore was chosen for further QSAR analysis. Figure 5 shows Pharm_A mapped onto the structures of NBMMPR, compound **4** and compound **25**. The three hydrogen bond acceptor features mapped onto the 3'-OH, the ribose ring oxygen, and the nitro group. The 3'-OH has been identified as an important structural feature for interaction with nucleoside transporters.^{18,38,39,40} The hydrophobic function is mapped onto the N^6 -benzyl ring, and the two aromatic groups are mapped onto the purine system. The importance of hydrophobicity of the purine 6-position substituent was highlighted in the study of Paul *et al.*²⁸

Compound **4** adopts an *anti* conformation, whereas compound **8** adopts a high-*anti* conformation due to the restriction imposed by the 5'-*O*, 8-linkage (see Figure 6). However, such a conformational shift is not large enough to prohibit compound **8** from mapping onto all

the chemical features encoded in the pharmacophore, which is consistent with the results obtained from the flow cytometric assay showing that compound **8** was able to bind well to the ENT1 transporter with a K_i values in the nanomolar range ($K_i = 18.89$ nM, see Table 3). Figure 7 shows that compounds **6**, **7**, and **9** are only partly mapped onto the pharmacophore with two or more encoded features being unmatched, which is consistent with the biological results as well (K_i values of compounds **6**, **7**, and **9** are all in the micromolar range, see Table 3). These findings suggest that the *anti*-conformation might be the optimal conformation for NBMPr and its analogues in binding to ENT1. Other factors may also contribute or be responsible for the low activity of these compounds such as unfavorable interactions of the region around the C^8 - $O^{5'}$ cyclic linkage. The reduced flexibility (lower entropy), possible atom bumping (unfavorable van der Waals), charge and/or hydrophobic/hydrophilic mismatch could also be the cause of the observed low binding affinity.

To further validate the Pharm_A pharmacophore hypothesis, a Pharm_A-dependent alignment of the training and test set compounds was exported to the SYBYL program and used for CoMFA 3D-QSAR modeling. The high sensitivity of CoMFA to molecular alignment led to elimination of compounds as outliers. All the conformationally constrained analogues of NBMPr, that we have synthesized, compounds **2–5**,¹ compound **26**, and compounds **6–9** were accommodated in the training set (see Fig. 8 for the alignments of training set and test set compounds used for the CoMFA 3D-QSAR derivation). The CoMFA model was developed with 57 compounds in the training set and afforded an r^2 of 0.894 and q^2 value of 0.591 (PLS statistics results of CoMFA model are shown in Table 7). To make sure that these results were not obtained by chance, PLS runs with scrambled (randomized) pIC_{50} values and group cross validations were performed (see Table 8). In the randomization control exercise, the majority of the analyses afforded very poor q^2 values, indicating that the CoMFA model generated with the actual data did not arise fortuitously. The deviations in the q^2 values resulting from the group cross-validations were minimal, suggesting the model is robust. The model was further validated by using it to predict the ENT1 inhibitory activities of an external test set of 39 compounds, and it showed a strong predictive ability, with a predictive r^2 of 0.73 (see Figure 9). Residuals of the predictions of the test set by the CoMFA 3D-QSAR model are shown in Table 9. The PLS coefficient contour maps depict regions around the molecules in 3D space where changes in physicochemical features increase or decrease potency as predicted (see Figure 10). The green colored areas denote regions that prefer sterically bulky groups in the CoMFA model, whereas yellow colored regions are sterically restricted. The blue contours indicate regions that favor electropositive substituents, whereas red contours mark regions favoring electronegative groups. As shown in Figure 10, a red region near the nitro group of NBMPr shows that an electronegative substituent at this site increases potency. This is consistent with the pharmacophore hypothesis (Pharm_A) in which the nitro group at this position is an H-bonding acceptor, and SAR studies that show high potencies for NBMPr, **27**, and **34** compared to their respective counterparts without nitro substitution, compounds **39**, **54**, and **29** (see Table 1). The green contour near the *para* position of the 6-benzyl ring indicates that generally a sterically bulky substituent is favored at this site; however, a yellow region is on the other side of the 6-benzyl group indicating that there is a limit as to the degree of bulkiness of the substituent at this region. The yellow contour near the *ortho* position of 6-benzyl group shows that the steric bulk around this region is disfavored. The blue contour near the purine ring shows that an electron deficient system is favored at this site. The pharmacophore map (Figs. 5 and 6) and CoMFA contour maps (Fig. 10) complement each other with the former appearing to capture more specific features than the latter. The results obtained from the CoMFA study further validated the Pharm_A hypothesis, suggesting that the *anti* conformation might be a possible bioactive conformation of NBMPr and its analogues.

Conclusion

In our continuing efforts to probe the bioactive conformation of NBMPR and its analogues at the ENT1 transporter, we carried out the synthesis and flow cytometric evaluation of new, more conformationally constrained analogues, combined them with our previous synthesized constrained analogues, as well as a diverse literature reported NBMPR congeners to derive a 3D pharmacophore model development of a bioactive conformation. CoMFA 3D-QSAR modeling was utilized in validation of this pharmacophore, which consists of three hydrogen bond acceptors, one hydrophobic group, and two aromatic rings, generated using the PHASE program. The use of a substantial number of compounds in both the training and the external test sets in the validation process, leads us to believe that the *anti* conformation indicated by this pharmacophore model, is a possible bioactive conformation of NBMPR at the ENT1 nucleoside transporter. This remains to be tested by experimental structural biology studies. The established CoMFA 3D-QSAR model of high predictive ability and robustness should be useful for the design and optimization and of new ENT1 inhibitors.

Experimental Section

Chemistry

Thin-layer chromatography (TLC) was conducted on silica gel F₂₅₄ plates (Analtech). Compounds were visualized by UV light or 5 % H₂SO₄ in EtOH spraying reagent. ¹H, ¹³C spectra were recorded on Bruker ARX (300 MHz) instruments, using CDCl₃, CD₃OD, (CD₃)₂SO or CD₃COCD₃ as solvents and tetramethylsilane (TMS) as internal standard. Column chromatography was performed on Fisher silica gel (170–400 mesh). Melting points were determined using a Fisher-Johns Melting Point Apparatus and are reported uncorrected. Mass spectra were obtained on a Bruker-HP Esquire-LC mass spectrometer, and IR spectra in KBr with a Perkin Elmer (System 2000 FT-IR) spectrometer. All solvents and reagents were bought from Aldrich and used without further purification except drying when necessary. Purity of Compounds **7**, **8**, and **9** was checked with a Hewlett-Packard 1100 HPLC apparatus equipped with a Platinum EPS 100A 5 μ C18 analytical column (150 × 4.6 mm, Phenomenex, Torrance, CA) in a linear gradient solvent system, H₂O/CH₃CN from 100/0 to 20/80 in 30 min; the flow rate was 1 ml/min. Peaks were detected by UV absorption with a diode array detector.

General Method for the Preparation of Compounds **6**, **7**, **8**, and **9**

A mixture of 5'-O, 8-cyclo-6-chloropurine riboside (**17**, 100 mg, 0.35 mmol), Mono- (5, 6, 7, or 8)-NO₂-1, 2, 3, 4-tetrahydroisoquinoline (**21**, **22**, **23**, or **24**, 157 mg, 0.88 mmol), and calcium carbonate (70 mg, 0.7 mmol) in ethanol (5 ml) was stirred under refluxing for 15 h. The reaction mixture was filtered, and the filtrate was evaporated in vacuo at 40 °C. The residue was purified by flash silica gel chromatography followed by recrystallization from Methanol.

6-[[Mono- (5", 6", 7", or 8")-NO₂-] 1, 2, 3, 4-tetrahydroisoquino-2-yl]-5'-O, 8-cyclo-purine riboside (6–9)—Compound 6: yield 74 %; mp 250–252 °C; MS m/z 427 (M⁺ + H); ¹H NMR (300MHz, (CD₃)₂SO), δ 8.29 (1H, s, H-2), 7.87 (1H, d, *J* = 8.1 Hz, H-6"), 7.67 (1H, d, *J* = 7.5 Hz, H-8"), 7.48 (1H, t, *J* = 7.8 Hz, H-7"), 6.04 (1H, s, H-1'), 5.63 (1H, d, *J* = 6.6, OH-2', disappears on D₂O exchange), 5.36 (1H, d, *J* = 5.4 Hz, OH-3', disappears on D₂O exchange), 5.32 (2H, br s, H-1"), 4.63 (1H, d, *J* = 2.1, H-2'); 4.58 (1H, br d, H-5'A), 4.45 (1H, t, *J* = 5.4 Hz, H-3'); 4.36 (2H, br s, H-3"); 4.25 (1H, t, *J* = 6.6, H-5'B); 4.13 (1H, d, *J* = 12.6 Hz, H-4'); 3.10 (2H, t, *J* = 5.7 Hz, H-4"). Anal. Calcd. For C₁₉H₁₈N₆O₆ (426.39): C, 53.52%; H, 4.26%; N, 19.71%. Found: C, 53.18 %; H, 4.24 %; N, 19.31 %.

Compound 7: yield 74 %; mp 179–180 °C; MS m/z 427(M⁺ + H); ¹H NMR (300MHz, (CD₃)₂SO), δ 8.29 (1H, s, H-2), 8.09 (1H, s, H-5"); 8.05 (1H, d, *J* = 4.4 Hz, H-7"), 7.56 (1H,

d, $J = 8.1$ Hz, H-8''), 6.05 (1H, s, H-1'), 5.64 (1H, br s, OH-2', disappears upon D₂O exchange), 5.33 (3H, br s, H-1'', OH-3', simplifies on D₂O exchange), 4.63 (1H, m, H-2'); 4.58 (1H, br m, H-5'A), 4.45 (1H, m, H-3'); 4.36 (2H, br s, H-3''); 4.25 (1H, d, $J = 5.1$, H-5'B); 4.13 (1H, d, $J = 12.6$ Hz, H-4'); 3.06 (2H, t, $J = 5.4$ Hz, H-4''); HPLC 20.8 min (97 %).

Compound 8: yield 55%; mp 188–190°C; MS m/z 449($M^+ + Na$); ¹H NMR (300MHz, (CD₃)₂SO), δ 8.31 (1H, s, H-2), 8.20 (1H, s, H-8''); 8.07 (1H, d, $J = 7.5$ Hz, H-6''), 7.49 (1H, t, $J = 7.8$ Hz, H-5''), 6.07 (1H, s, H-1'), 5.65 (1H, d, $J = 6.6$, OH-2', disappears upon D₂O exchange), 5.38 (1H, d, $J = 5.4$ Hz, OH-3', simplifies upon D₂O exchange), 5.33 (2H, br s, H-1''), 4.66 (1H, d, $J = 2.1$, H-2'); 4.59 (1H, br d, H-5'A), 4.47 (1H, t, $J = 5.4$ Hz, H-3'); 4.43 (2H, br s, H-3''); 4.25 (1H, t, $J = 6.6$, H-5'B); 4.13 (1H, d, $J = 12.6$ Hz, H-4'); 3.05 (2H, t, $J = 5.7$ Hz, H-4''); HPLC 23.9 min (95 %).

Compound 9: yield 47 %; mp 171–172°C; MS m/z 449($M^+ + Na$); ¹H NMR (300MHz, (CD₃)₂SO), δ 8.28 (1H, s, H-2), 7.94 (1H, d, $J = 8.1$ Hz, H-7''); 7.58 (1H, d, $J = 6.9$ Hz, H-5''), 7.46 (1H, t, $J = 7.8$ Hz, H-6''), 6.03 (1H, s, H-1'), 5.62 (1H, d, $J = 6.6$, OH-2', disappears on D₂O exchange), 5.55 (2H, br s H-1''), 5.36 (1H, d, $J = 5.4$ Hz, OH-3', disappears upon D₂O exchange), 4.63 (1H, d, $J = 2.4$, H-2'); 4.58 (1H, br d, H-5'A), 4.44 (1H, t, $J = 5.7$ Hz, H-3'); 4.37 (2H, br s, H-3''); 4.22 (1H, t, $J = 6.3$, H-5'B); 4.12 (1H, d, $J = 12.9$ Hz, H-4'); 3.04 (2H, t, $J = 5.7$ Hz, H-4''); HPLC 21.1 min (99 %).

6-(7''-NO₂ - 1, 2, 3, 4-tetrahydroisoquino-2-yl)-2', 3'-O-*p*-isopropylidene purine riboside (10)—To a suspension of 6-(7''-NO₂ - 1, 2, 3, 4-tetrahydroisoquino-2-yl) purine riboside (**4**, 1.11g, 2.6 mmol) in 30 ml of acetone was added 0.4 ml of 70 % HClO₄ at 0 °C. The reaction mixture was stirred overnight at room temperature, after which the reaction mixture was neutralized with NH₃·H₂O and evaporated to dryness under aspirator pressure at 40 °C. The crude product was recrystallized from ethanol to give 1.14 g of 6-(7''-NO₂ - 1, 2, 3, 4-tetrahydroisoquino-2-yl)-2', 3'-O-*p*-isopropylidene purine riboside (**10**) (94 % yield). mp 88–90 °C; MS m/z 469($M^+ + H$); ¹H NMR (300MHz, CDCl₃), δ 8.36 (1H, s, H-2), 8.16 (1H, s, H-8''); 8.08 (1H, d, $J = 7.8$ Hz, H-6''), 7.35 (1H, t, $J = 7.8$ Hz, H-5''), 6.70 (1H, d, $J = 6.0$ Hz, OH-5', disappeared upon D₂O exchange); 5.85 (1H, d, $J = 5.4$ H-1'), 5.52 (2H, br s, H-1''), 5.25 (1H, t, $J = 5.4$, H-2'); 5.14 (1H, t, $J = 5.4$ Hz, H-3'); 4.58 (3H, br d, H-3'', H-5'A), 4.0 (1H, d, $J = 12.6$ Hz, H-4'); 3.80 (1H, t, $J = 6.6$, H-5'B); 3.12 (2H, t, $J = 5.7$ Hz, H-4''). 1.66 (3H, s, CH₃ of isopropylidene group); 1.38 (3H, s, CH₃ of isopropylidene group).

6-(7''-NO₂ - 1, 2, 3, 4-tetrahydroisoquino-2-yl)-2', 3'-O-*p*-isopropylidene-8-OH purine riboside (13)—6-(7''-NO₂ - 1, 2, 3, 4-tetrahydroisoquino-2-yl)-2', 3'-O-*p*-isopropylidene purine riboside (**10**, 500 mg, 1.07 mmol) was dissolved in a mixture of dioxane and 10 % disodium hydrogen phosphate buffer (32 ml, 1:1, vol/vol), then bromine (204.7 mg, 1.28 mmol) was added while stirring. The reaction mixture was stirred for 20 hours at ambient temperature, followed by the addition of 2N NaHSO₃ to reduce the excess bromine. The solution was extracted with CH₂Cl₂. The combined organic layer was washed with 2N NaHSO₃, dried over Na₂SO₄, and evaporated to give sticky residue, which was purified on preparative TLC plates using MeOH/EtOAc mixture (1:20 v/v) as the solvent system to afford **13** (156 mg, 30 % yield). mp 228–230°C; MS m/z 484($M^+ + H$); ¹H NMR (300MHz, CDCl₃), δ 8.98 (1H, s, H-2), 8.58 (2H, br s, H-8'', OH-8, simplifies on D₂O exchange); 8.38 (1H, d, $J = 7.8$ Hz, H-6''), 7.54 (1H, t, $J = 7.8$ Hz, H-5''), 6.32 (1H, s, H-1'), 5.49 (1H, d, $J = 5.4$, H-2'); 5.12 (1H, m, H-3'), 4.45 (4H, m, H-1'', 3''); 3.65 (1H, t, $J = 6.6$, H-5'A); 3.45 (1H, m, H-4'); 3.30 (3H, m, H-4'', H-5'B); 1.40 (3H, s, CH₃ of isopropylidene group); 1.25 (3H, s, CH₃ of isopropylidene group).

2', 3'-O-isopropylidene-6-chloropurine riboside (15)—A suspension of 6-chloro purine riboside (**14**, 1.0g, 3.5 mmol) in 42 ml of acetone was stirred overnight with 0.6ml of

70 % HClO₄ at room temperature. The reaction mixture was neutralized with NH₃·H₂O, after which the mixture was evaporated to dryness under aspirator pressure at 40°C. The crude product was recrystallized from ethanol to give 1.1 g of 6-(7''-NO₂-1, 2, 3, 4-tetrahydroisoquino-2-yl)-2', 3'-*O*-*p*-isopropylidene purine riboside (**15**) (94 % yield). mp 160–161 °C; MS m/z 449(M⁺ + Na); ¹H NMR (300MHz, CDCl₃), δ 8.80 (1H, s, H-8); 8.26 (1H, s, H-2), 5.98 (1H, d, *J* = 5.4 Hz, H-1'); 5.22 (1H, t, *J* = 5.4, H-2'); 5.14 (1H, t, *J* = 5.4 Hz, H-3'); 4.96 (1H, dd, *J* = 6.0, 2.1 Hz, OH-5', disappeared upon D₂O exchange); 4.58 (1H, br s, H-4'); 4.0 (1H, d, *J* = 7.8 Hz, H-5'A); 3.84 (1H, t, *J* = 6.6, H-5'B); 1.68 (3H, s, CH₃ of isopropylidene group); 1.42 (3H, s, CH₃ of isopropylidene group).

5'-*O*, 8-cyclo-2', 3'-*O*- isopropylidene-6-chloropurine riboside (16)—A mixture of 2', 3'-*O*-isopropylidene-6-chloropurine riboside (**15**) (960 mg, 2.94 mmol) and *N*-iodosuccinimide (NIS) (2.01g, 8.8 mmol) in acetic acid (29 ml) was stirred at 50–60 °C for 3 days. Acetic acid was removed in vacuo. The concentrated reaction mixture was neutralized with NH₃·H₂O and extracted with ethyl acetate (30 ml × 3). The organic layer was separated and washed with water (10 ml × 3), dried over anhydrous Na₂SO₄ and evaporated. The residue was subjected to chromatography on silica gel eluting with Hexane/EtOAc (3:2) to provide 344 mg of 5'-*O*, 8-cyclo-2', 3'-*O*-*p*-anisylidene-6-chloropurine riboside (**16**) as crystals (36 %). mp 224–226 °C; MS (ESI) m/z 347 (M⁺ + Na); ¹H NMR (300 MHz, CDCl₃), δ 8.62 (1H, s, H-2), 6.44 (1H, s, H-1'), 5.08 (1H, d, *J* = 5.4, H-4'), 4.70 (2H, m, H-5'), 4.52 (1H, d, *J* = 6.0 Hz, H-3'), 4.24 (1H, d, *J* = 6.0 Hz, H-2'), 2.12 (3H, s, CH₃ of isopropylidene group); 1.32 (3H, s, CH₃ of isopropylidene group).

2', 3'-*O*- isopropylidene-8-hydroxy-6-chloropurine riboside (18)—5'-*O*, 8-cyclo-2', 3'-*O*- isopropylidene-6-chloropurine riboside (**16**, 100 mg, 0.31 mmol) was suspended in 0.5 N H₂SO₄ (4 ml) and stirred at 55°C for 15 h. The reaction mixture was neutralized with NH₃·H₂O and evaporated to dryness in vacuo. The residue was subjected to chromatography on preparative TLC plates using a mixture of MeOH/EtOAc (1:20) as the solvent system. The purified product was characterized as 8-hydroxy-2', 3'-*O*- isopropylidene-6-chloropurine riboside (**18**) (23.3 mg, 25 % yield). MS (ESI) m/z 325(M⁺ + Na); ¹H NMR (300MHz, (CD₃)₂SO), δ 12.31 (1H, br s, OH-8); 8.48 (1H, s, H-2), 5.73 (1H, d, *J* = 6.4 Hz, H-1'), 5.31 (1H, d, *J* = 6.6, OH-2'), 5.12 (1H, d, *J* = 5.7 Hz, OH-3'), 4.89 (1H, q, *J* = 10.8 Hz, H-2'), 4.76 (1H, t, *J* = 6.6 Hz, OH-5'); 4.21 (1H, t, *J* = 6.0 Hz, H-3'); 3.86 (1H, t, *J* = 6.0 Hz, H-4'); 3.62 (1H, m, H-5'A); 3.48 (1H, m, H-5'B).

2', 3'-*O*-*p*-anisylidene-6-chloropurine riboside (19)—A suspension of zinc chloride (2.65 g, 19.4 mmol) in *p*-methoxybenzaldehyde (10 ml) was stirred for 30 min at 30–40 °C, and then 6-chloropurine riboside (**14**) (1 g, 3.5 mmol) was added. The mixture was stirred at room temperature for 5 days. The semi-solid product was poured on ice and extracted with CHCl₃ (40 ml × 3) and the combined organic extracts was washed with water, dried over anhydrous Na₂SO₄ and evaporated. The residue was chromatographed on silica gel. Eluate of 60 % ethyl acetate in hexane was collected and evaporated to give Compound **19** (1.2g, 81 %). mp 128–130 °C; MS (ESI) m/z 427(M⁺ + Na); ¹H NMR (300MHz, (CD₃)₂SO), a 2:1 mixture of stereoisomers doubling most signals, δ 8.92 (1H, s, H-8), 8.84 (1H, s, H-2), 7.45 (2H, d, *J* = 9.0 Hz, ortho-H of *p*-anisylidene ring), 6.88 (2H, d, *J* = 9.0 Hz, para-H of *p*-anisylidene ring), 6.45 (1H, d, *J* = 3.0 Hz, H-1'), 6.21 (1H, s, *p*-anisylidene CH), 5.52 (1H, m, H-2'), 5.15 (1H, t, *J* = 6.0 Hz, OH-5'), 5.12 (1H, m, H-3'), 4.38 (1H, q, *J* = 6.0 Hz, H-4'), 3.78 (3H, s, OCH₃), 3.63 (2H, m, H-5'). Anal. Calcd. For C₁₈H₁₇ClN₄O₅ (404.81): C, 53.41%; H, 4.23%; Cl, 8.76%, N, 13.84%. Found: C, 53.27%; H, 4.23%; Cl, 8.64%, N, 13.76%.

5'-*O*, 8-cyclo-2', 3'-*O*-*p*-anisylidene-6-chloropurine riboside (20)—A mixture of 2', 3'-*O*-*p*-anisylidene-6-chloropurine riboside (**19**) (1.0g, 2.48 mmol) and *N*-iodosuccinimide

(NIS) (1.6 g, 7.4 mmol) in acetic acid (24 ml) was stirred at ambient temperature for 3 days. Acetic acid was removed in vacuo. The concentrated reaction mixture was neutralized with $\text{NH}_3\cdot\text{H}_2\text{O}$ and extracted with ethyl acetate (30 ml \times 3). The organic layer was separated and washed with water, dried over anhydrous Na_2SO_4 and evaporated. The residue was subjected to chromatography on SiO_2 and eluted with Hexane/EtOAc mixture (1:1) to provide 429 mg of 5'-O, 8-cyclo-2', 3'-O-*p*-anisylidene-6-chloropurine riboside (**20**) as a crystal (yield 43 %). mp 215–216 °C; MS (ESI) m/z 425($\text{M}^+ + \text{Na}$); ^1H NMR (300MHz, CDCl_3), δ 8.71 (1H, s, H-2), 7.40 (2H, d, $J = 9.0$ Hz, ortho-H of *p*-anisylidene ring), 6.94 (2H, d, $J = 9.0$ Hz, para-H of *p*-anisylidene ring), 6.67 (1H, s, H-1'), 6.19 (1H, s, *p*-anisylidene CH), 5.25 (1H, d, $J = 6.0$, H-2'), 4.92 (2H, q, $J = 9.0$ Hz, H-5'), 4.69 (1H, q, $J = 9.0$ Hz, H-3'), 4.31 (1H, d, $J = 12.0$ Hz, H-4'), 3.83 (3H, s, OCH_3). Anal. Calcd. For $\text{C}_{18}\text{H}_{15}\text{ClN}_4\text{O}_5$ (402.80): C, 53.67%; H, 3.75%; N, 13.91%. Found: C, 53.23 %; H, 3.77 %; N, 13.68 %.

5'-O, 8-cyclo-6-chloropurine riboside (17)—5'-O, 8-cyclo-2', 3'-O-*p*-anisylidene-6-chloropurine riboside (**20**) (320 mg, 0.8 mmol) was suspended in 80 % trifluoroacetic acid (4 ml) and stirred in an ice bath for 4 hours. The reaction mixture was neutralized with $\text{NH}_3\cdot\text{H}_2\text{O}$ and evaporated in vacuo to remove water. The resulting residue was dissolved in ethyl acetate and subjected to chromatography on silica gel using a mixture of Hexane/EtOAc (1:4) as eluant to give 166 mg of 5'-O, 8-cyclo-6-chloropurine riboside (**17**) as crystals (73 %). mp 212–213 °C; MS (ESI) m/z 307($\text{M}^+ + \text{Na}$); ^1H NMR (300MHz, $(\text{CD}_3)_2\text{SO}$), δ 8.71 (1H, s, H-2), 6.12 (1H, s, H-1'), 5.65 (1H, d, $J = 6.6$, OH-2'), 5.43 (1H, d, $J = 5.7$ Hz, OH-3'), 4.74 (1H, q, $J = 10.8$ Hz, H-2'), 4.64 (1H, br s, H-5'A), 4.46 (1H, t, $J = 6.0$ Hz, H-3'); 4.33 (1H, br d, $J = 6.0$ Hz, H-5'B); 4.29 (1H, br d, $J = 4.8$ Hz, H-4'). Anal. Calcd. For $\text{C}_{10}\text{H}_9\text{ClN}_4\text{O}_4$ (284.66): C, 42.19%; H, 3.19%; Cl, 12.45%; N, 19.68%. Found: C, 42.25 %; H, 3.30 %; Cl, 12.09; N, 19.33 %.

Biological Testing

The compounds were tested to determine their ENT1 (*es*) nucleoside transporter binding affinity by a flow cytometric assay (Buolamwini *et al.*, 1994). Human leukemia K562 cells growing in RPMI 1640 medium were washed once and suspended at 1.6×10^6 cells/ml in phosphate-buffered saline at pH 7.4, and incubated with 5-(SAENTA)-X8-fluorescein (25 nM) in the presence or absence of varying concentrations of test compounds at room temperature for 45 minutes. Flow cytometric measurements for cell-associated fluorescence were then performed on a FACSCalibur instrument (Becton Dickinson, San Jose, CA) equipped with a 15 mW-argon laser (Molecular Resources Flow Cytometry Facility, University of Tennessee Health Sciences Center). In each assay, 5,000 cells were analyzed from suspensions of 4×10^5 cells/ml. The units of fluorescence were arbitrary channel numbers. Percentage (%) of control (i.e. ENT1 transporter-specific fluorescence in the presence of SAENTA-fluorescein without test compounds) was calculated for each sample by the equation below:

$$\% \text{ Control} = \frac{(\text{SF}_s)}{(\text{SF}_f)} \times 100 \quad \text{Eq. 2}$$

where SF_s is the ENT1 transporter-specific fluorescence of test samples, and SF_f is the ENT1 transporter-specific fluorescence of the SAENTA-fluorescein ligand standard in mean channel numbers. Inhibition constants were calculated from the IC_{50} values K_i values using Eq. 3.

$$K_i = \text{IC}_{50} / (1 + [\text{L}] / K_L) \quad \text{Eq. 3}$$

where [L] and K_L are the concentration and the K_d value of the SAENTA-fluorescence, respectively. The results were fed into the PRISM program (GraphPad, San Diego, CA) to derive concentration-dependent curves, as shown in Figure 3. From these curves, the IC_{50} values were obtained and used to calculate K_i values, which were used to compare the abilities of compounds to displace the ENT1 (*es*) transporter-specific ligand, 5- (SAENTA)-X8-fluorescein (Buolamwini *et al.*, 1994), and for that matter their affinity for the transporter.

Acknowledgments

Financial support from the National Heart Lung and Blood Institute, grant number K01-HL067479 awarded to J.K.B. is gratefully acknowledged.

References

1. Zhu Z, Furr J, Buolamwini JK. *J Med Chem* 2003;46:831–837. [PubMed: 12593662]
2. Abd-Elfattah AS, Wechsler AS. *J Card Surg* 1994;9:387–396. [PubMed: 8069025]
3. Abd-Elfattah AS, Jessen ME, Lekven J, Wechsler AS. *Mol Cell Biochem* 1998;180:179–191. [PubMed: 9546645]
4. Van Belle H. *Cardiovasc Res* 27;1993:68–76.
5. Deckert J, Morgan PF, Marangos PJ. *Life Sci* 1988;42:1331–1345. [PubMed: 3280937]
6. Geiger, JD.; Parkinson, FE.; Kowaluk, EA. Regulators of endogenous adenosine levels as therapeutic agents. In: Jacobson, KA.; Jarvis, MF., editors. *Purinergic Approaches in Experimental Therapeutics*. Wiley-Liss; New York: 1997.
7. Ohta A, Sitkovsky M. *Nature* 2001;414:916–920. [PubMed: 11780065]
8. Weinstein GD, Jeffes E, McCullough JL. *J Invest Dermatol* 1990;95:49S–52S.
9. Hendrix CW, Flexner C, Szebeni J, Kuwahara S, Pennypacker S, Weinstein JN, Lietman PS. *Antimicrob Agents Chemother* 1994;38:1036–1040. [PubMed: 8067734]
10. Adjei AA, Dagnino L, Wong MM, Paterson AR. *Cancer Chemother Pharmacol* 1992;31:71–75. [PubMed: 1458562]
11. Dagnino L, Paterson AR. *Cancer Res* 50:6549–6553. [PubMed: 1698538]
12. Tew, KD.; Houghton, PJ.; Houghton, JA. Preclinical and clinical modulation of Anticancer Drugs. Vol. Chap. 7. CRC Press; Boca Raton: 1993. 1990
13. el Kouni MH. *Pharmacol Ther* 2003;99:283–309. [PubMed: 12951162]
14. Al Safarjalani ON, Naguib FN, el Kouni MH. *Antimicrob Agents Chemother* 2003;47:3247–3251. [PubMed: 14506037]
15. Yadav V, Chu CK, Rais RH, Al Safarjalani ON, Guarcello V, Naguib FN, el Kouni MH. *J Med Chem* 47;2004:1987–1996.
16. Williams EF. *SAAS Bull Biochem Biotechnol* 1996;9:51–56. [PubMed: 8652132]
17. Hoehner J, Wechsler AS, Abd-Elfattah AS. *Dev Cardiovasc Med* 1996;181:209–218.
18. Buolamwini JK. *Curr Med Chem* 1997;4:35–66.
19. Cass, CE. *Drug Transport in Antimicrobial and Anticancer Chemotherapy*. Georgopapadakou, NH., editor. Marcel Dekker; New York: 1995.
20. Sprague, PW. *Perspectives in Drug Discovery and Design*. ESCOM; Leiden: 1995. De Novo Design.
21. Nomenclature Committee of IUB (NC-IUB) and IUPAC-IUB Joint Commission on Biochemical Nomenclature (JCBN) . *Eur J Biochem* 1981;114:1–4. [PubMed: 7215345]Newsletter
22. Ikehara M, Uesugi S, Yasumoto MA. *J Am Chem Soc* 1970;92:4735–4736. [PubMed: 5428881]
23. Ikehara M, Tada H, Kaneko M. *Tetrahedron* 1968;24:3489–3498. [PubMed: 4171891]
24. Ikehara M, Kaneko M. *Tetrahedron* 1970;26:4251–4259. [PubMed: 5469477]
25. Lin TS, Cheng JC, Ishiguro K, Sartorelli AC. *J Med Chem* 1985;28:1481–1485. [PubMed: 3862866]
26. Kitade Y, Makino T, Hirota K, Maki Y. *Nucleosides Nucleotides* 1992;11:365–372.
27. Maki Y, Sako M, Saito T, Hirota K. *Heterocycles* 1988;27:347–350.
28. Paul B, Chen MF, Paterson AR. *J Med Chem* 1975;18:968–973. [PubMed: 1159691]

29. Robins MJ, Asakura J, Kanekc M, Shibuya S, Jakobs ES, Agbanyo FR, Cass CE, Paterson ARP. *Nucleosides Nucleotides* 1994;13:1627–1646.
30. Gupte A, Buolamwini JK. *Bioorg Med Chem Lett* 2004;14:2257–2260. [PubMed: 15081020]
31. Gupte A, Buolamwini JK, Yadav V, Chu CK, Naguib FN, el Kouni MH. *Biochem Pharmacol* 2005;71:69–73. [PubMed: 16310172]
32. Soriano-Garcia M, Parthasarathy R, Paul B, Paterson ARP. *Acta Cryst* 1984;C40:1897–1901.
33. Paterson AR, Naik SR, Cass CE. *Mol Pharmacol* 1977;13:1014–1023. [PubMed: 593261]
34. Buolamwini JK, Barchi JJ Jr. *Nucleosides Nucleotides* 1997;16:2101–2110.
35. Buolamwini JK, Wiley JS, Robins MJ, Craik JD, Cass CE, Gati WP, Paterson ARP. *Nucleosides Nucleotides* 1994;13:737–751.
36. Cramer RD III, Patterson DE, Bunce JD. *J Am Chem Soc* 1988;110:5959–5967.
37. Kubinyi, H., editor. *3D QSAR in Drug Design: Theory, Methods and Applications*. ESCOM Science Publishers; Leiden: 1993.
38. Chang C, Swaan PW, Ngo LY, Lum PY, Patil SD, Unadkat JD. *Mol Pharmacol* 2004;65:558–570. [PubMed: 14978234]
39. Zhang J, Smith KM, Tackaberry T, Visser F, Robins MJ, Nielsen LP, Nowak I, Karpinski E, Baldwin SA, Young JD, Cass CE. *Mol Pharmacol* 2005;68:830–9. [PubMed: 15955867]
40. Zhang J, Visser F, Vickers MF, Lang T, Robins MJ, Nielsen LP, Nowak I, Baldwin SA, Young JD, Cass CE. *Mol Pharmacol* 2003;64:1512–20. [PubMed: 14645682]

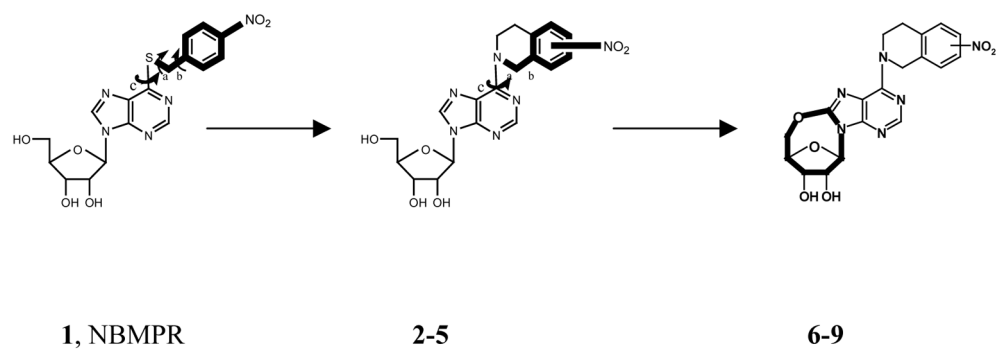


Figure 1.
Design of conformationally constrained analogues of NBMMPR.

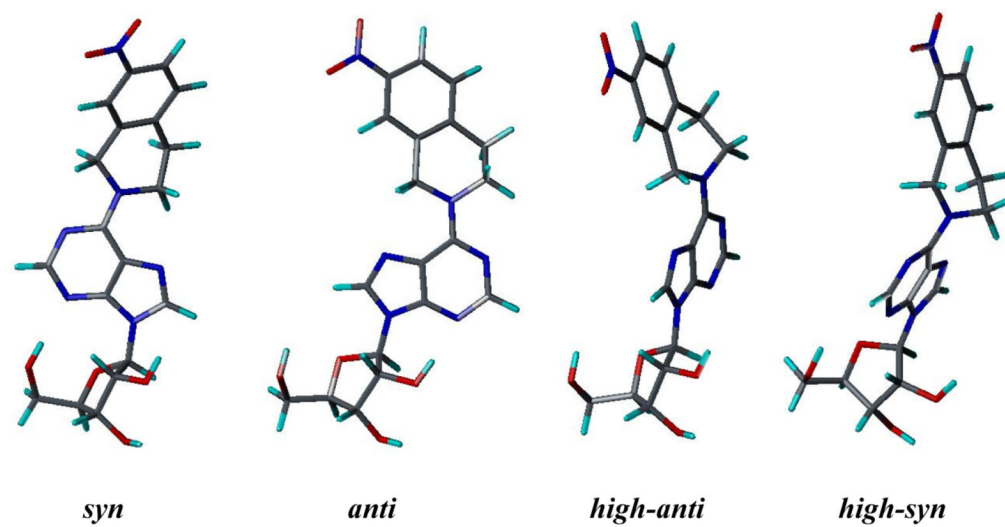


Figure 2. Different conformations of Compound 4 generated by rotation of the N^9-C1' glycosidic bond.

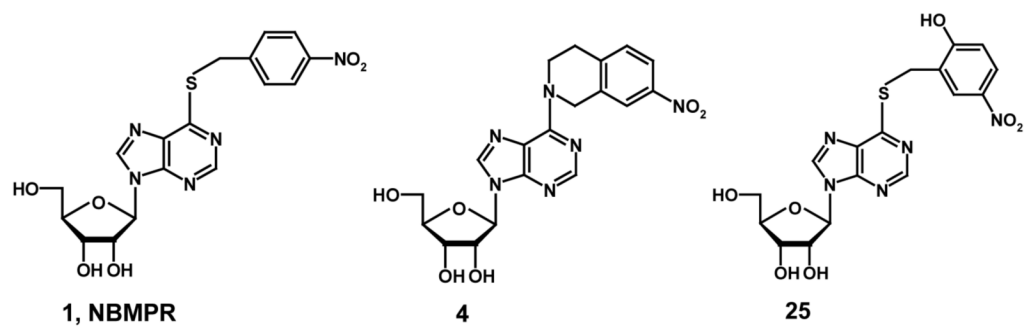


Figure 3. Active compounds used to generate common pharmacophore hypotheses in the PHASE program.

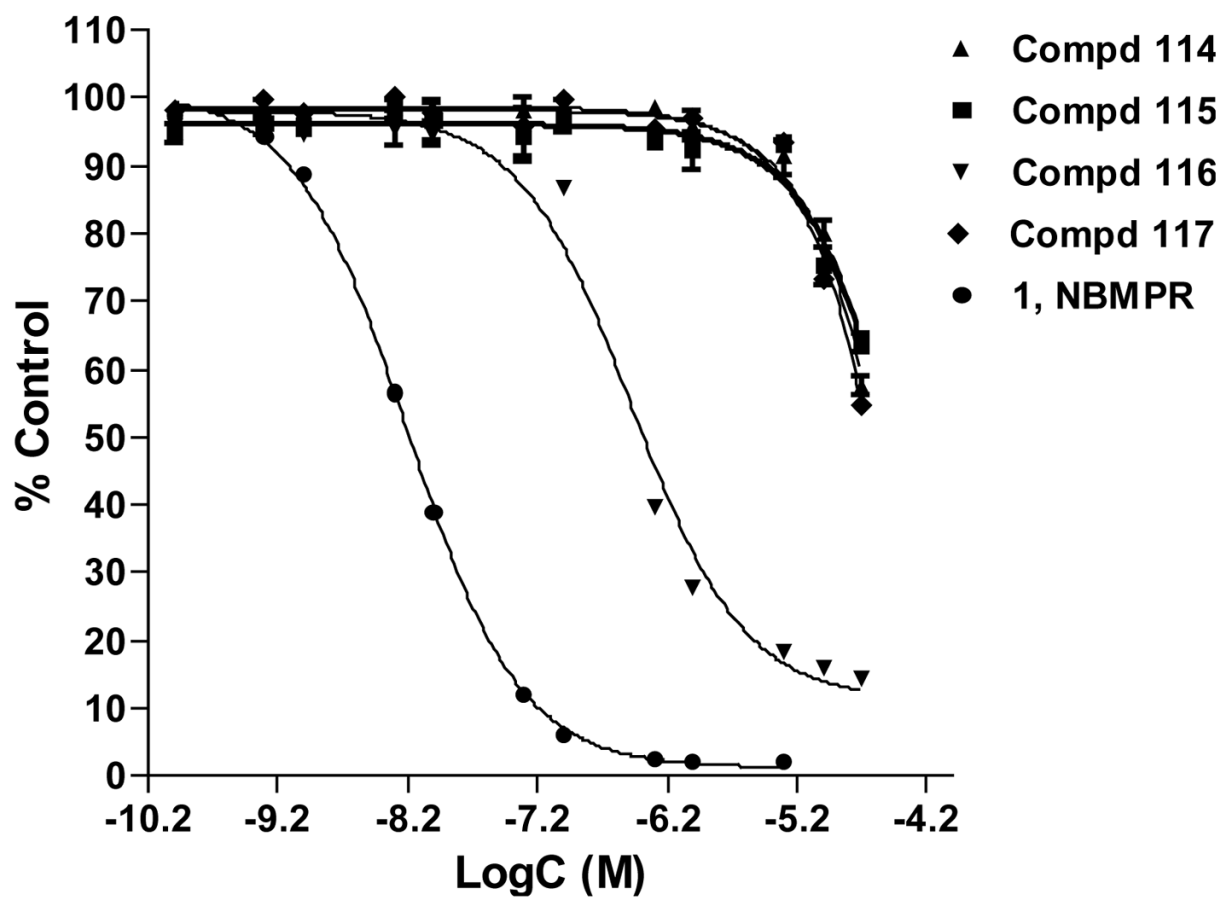


Figure 4. Equilibrium displacement of SAENTA-fluorescein by compounds **6–9**, the 5'-O, 8-cyclo highly conformationally constrained analogues of NBMPR, in K562 cells.

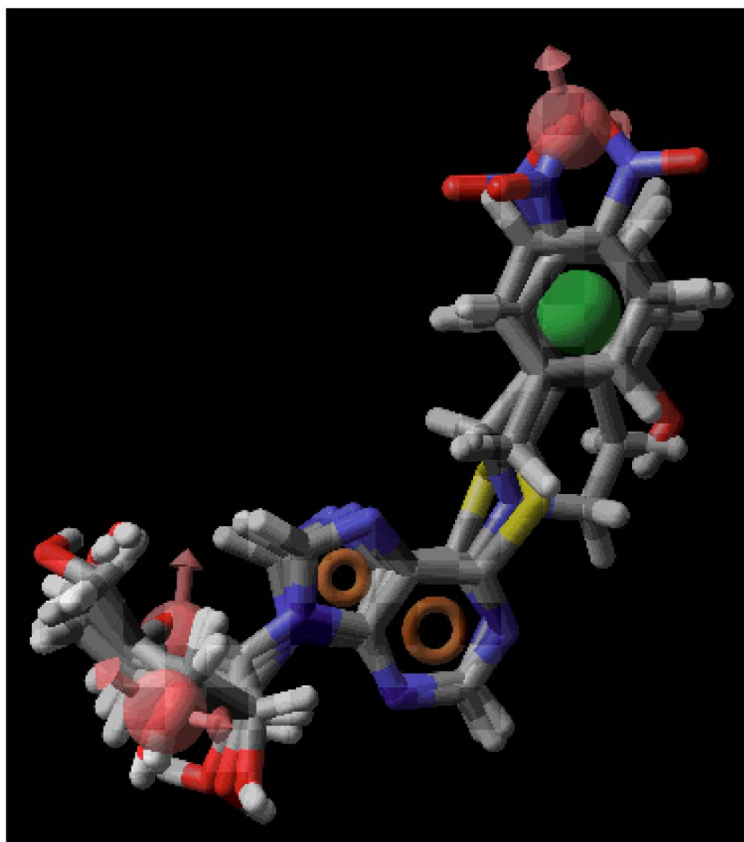


Figure 5.

The best-generated pharmacophore model (Pharm_A) obtained from PHASE. Pharmacophore features are red vectors for hydrogen bond acceptors (A), orange rings for aromatic groups (R), and green balls for hydrophobic functions (H). NBMPR, compound **4**, and compound **25** were aligned to the pharmacophore. For the molecules, blue indicates nitrogen, red indicates oxygen, yellow refers to sulfur, gray indicates carbon, and white indicates hydrogen.

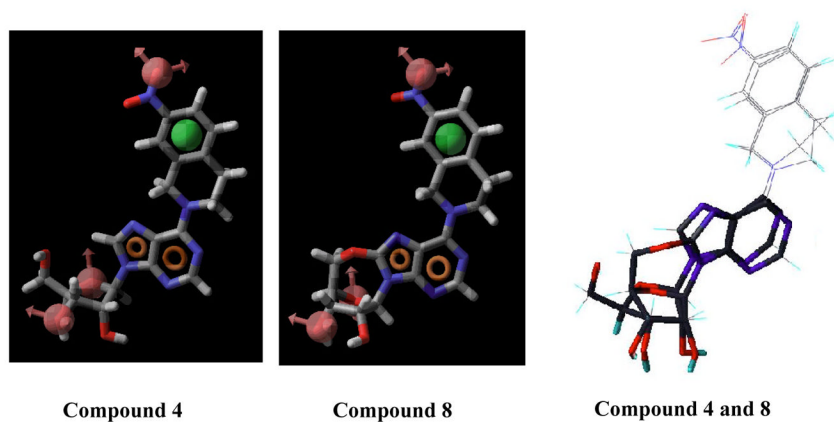


Figure 6. Pharmacophore feature mapping onto compounds **4** and **8** and their conformational comparison. Pharmacophore features are red vectors for hydrogen bond acceptors (A), orange rings for aromatic groups (R), and green balls for hydrophobic functions (H). NBMPR, compound **4**, and compound **25** were aligned to the pharmacophore. Molecules are blue for nitrogen, red for oxygen, yellow for sulfur, gray for carbon, and white for hydrogen.

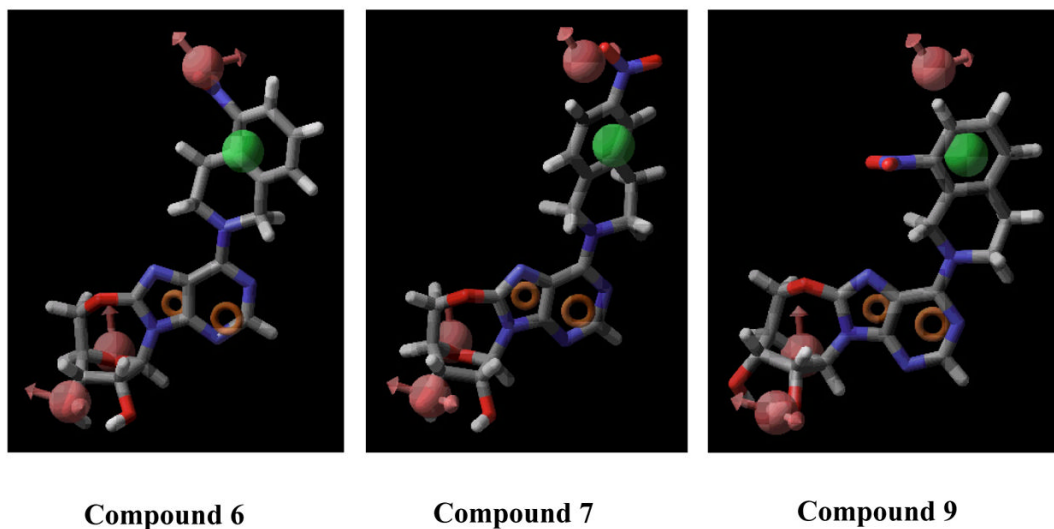


Figure 7.

Pharmacophore feature mapping onto compounds **6**, **7**, and **9**. Pharmacophore features are red vectors for hydrogen bond acceptors (A), orange rings for aromatic groups (R), and green balls for hydrophobic functions (H). NBMPR, Compound **4**, and Compound **25** were aligned to the pharmacophore. For the molecules, blue indicates nitrogen, red indicates oxygen, yellow refers to sulfur, gray indicates carbon, and white indicates hydrogen.

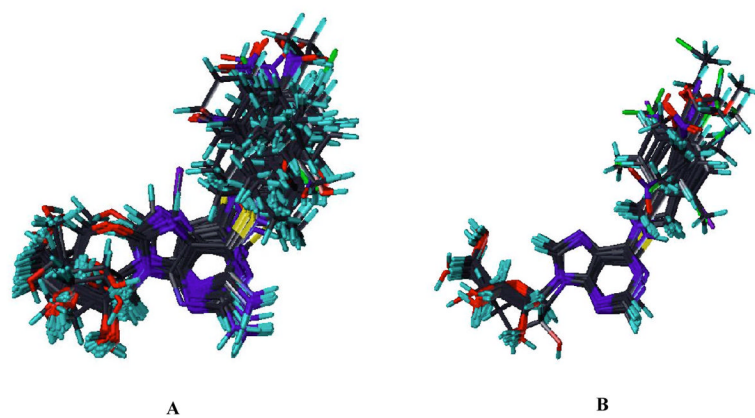


Figure 8. Superimposition of training set (A) and test set (B) aligned to the pharmacophore model, Pharm_A, imported from PHASE.

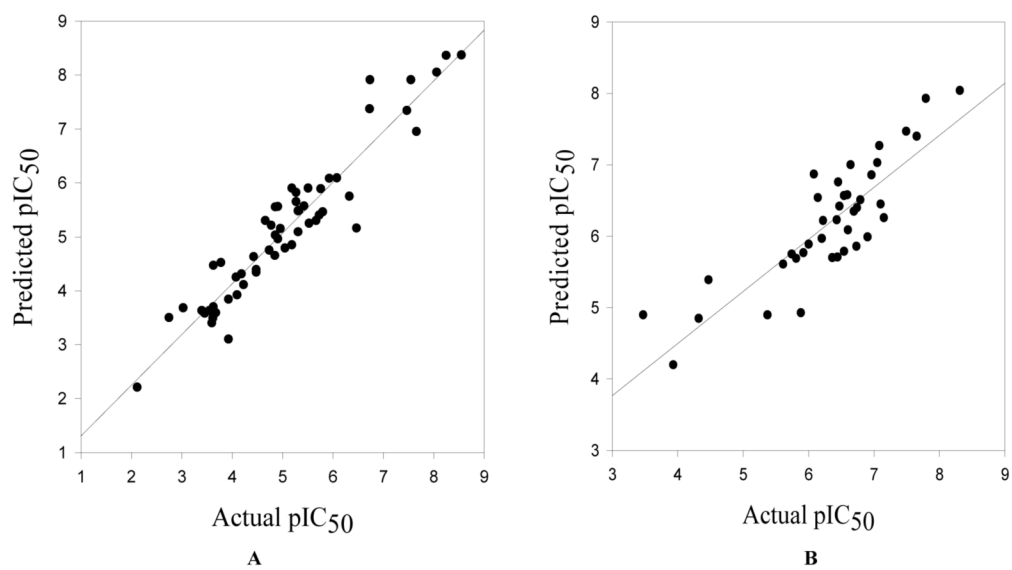


Figure 9. Curves for training set (A) and test set (B) activity predictions by the CoMFA 3D QSAR model.

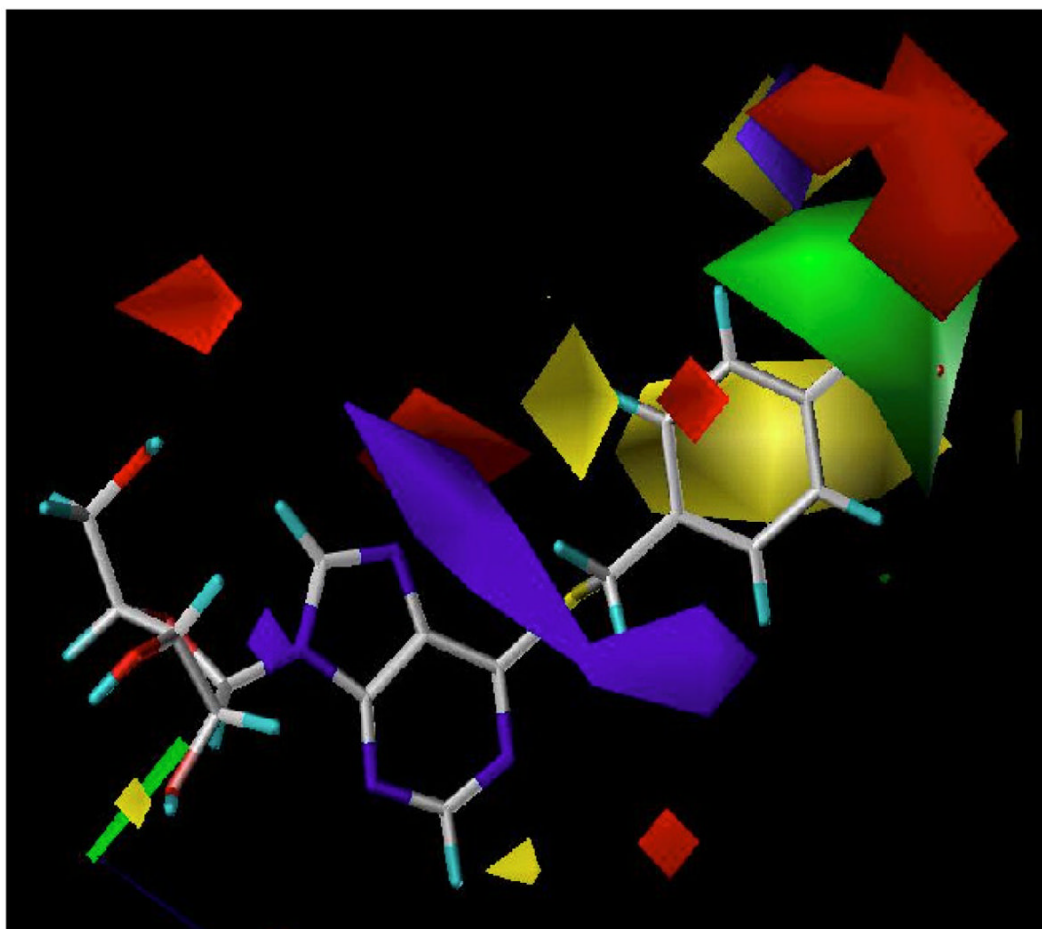
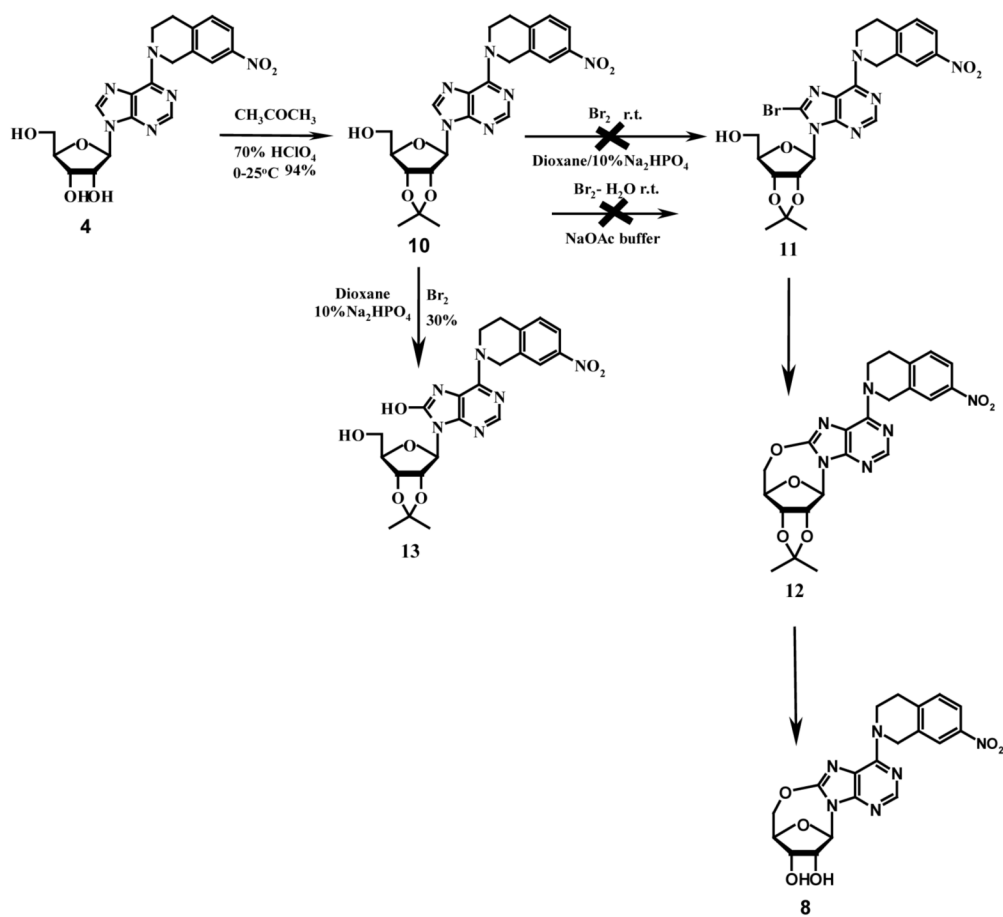
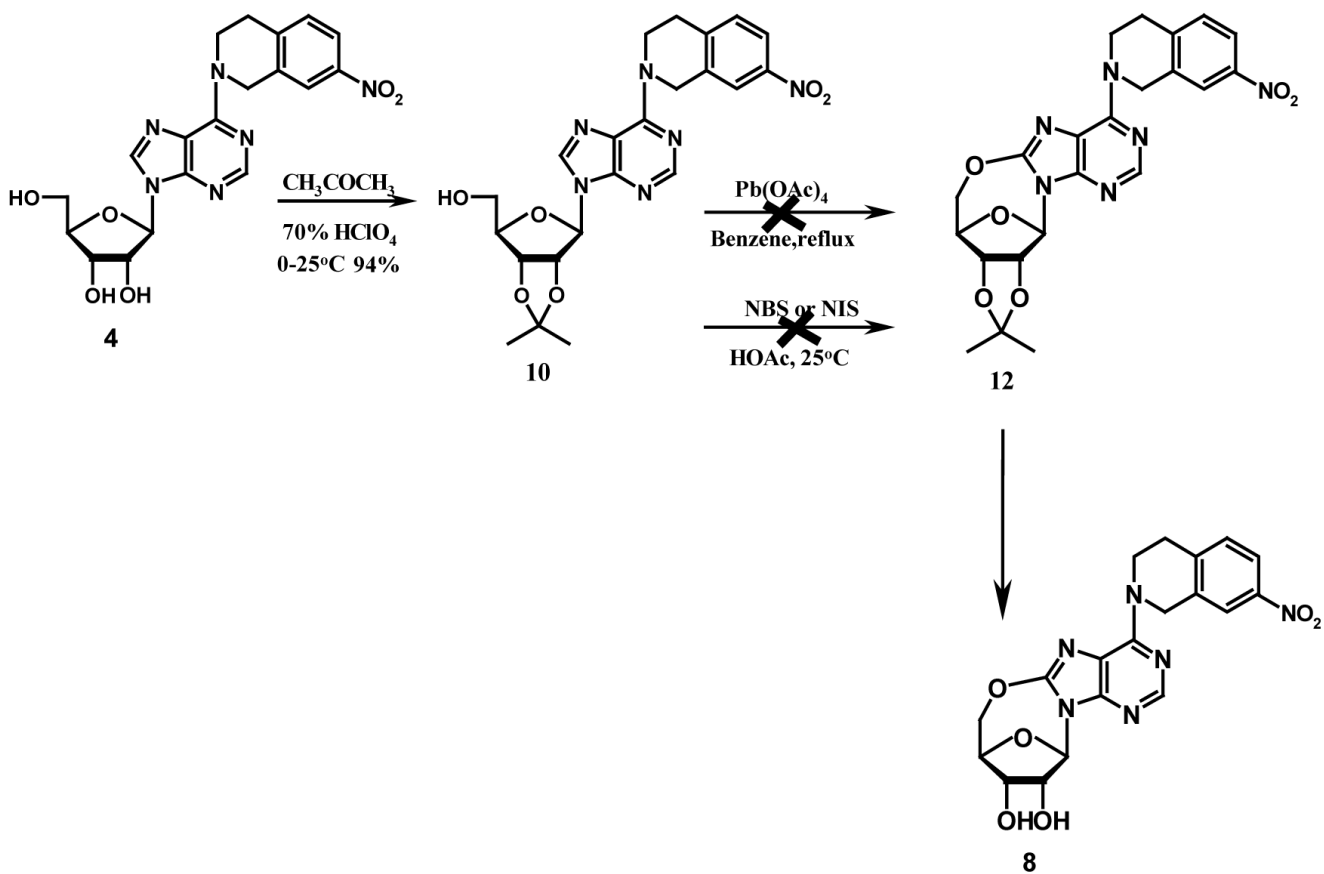


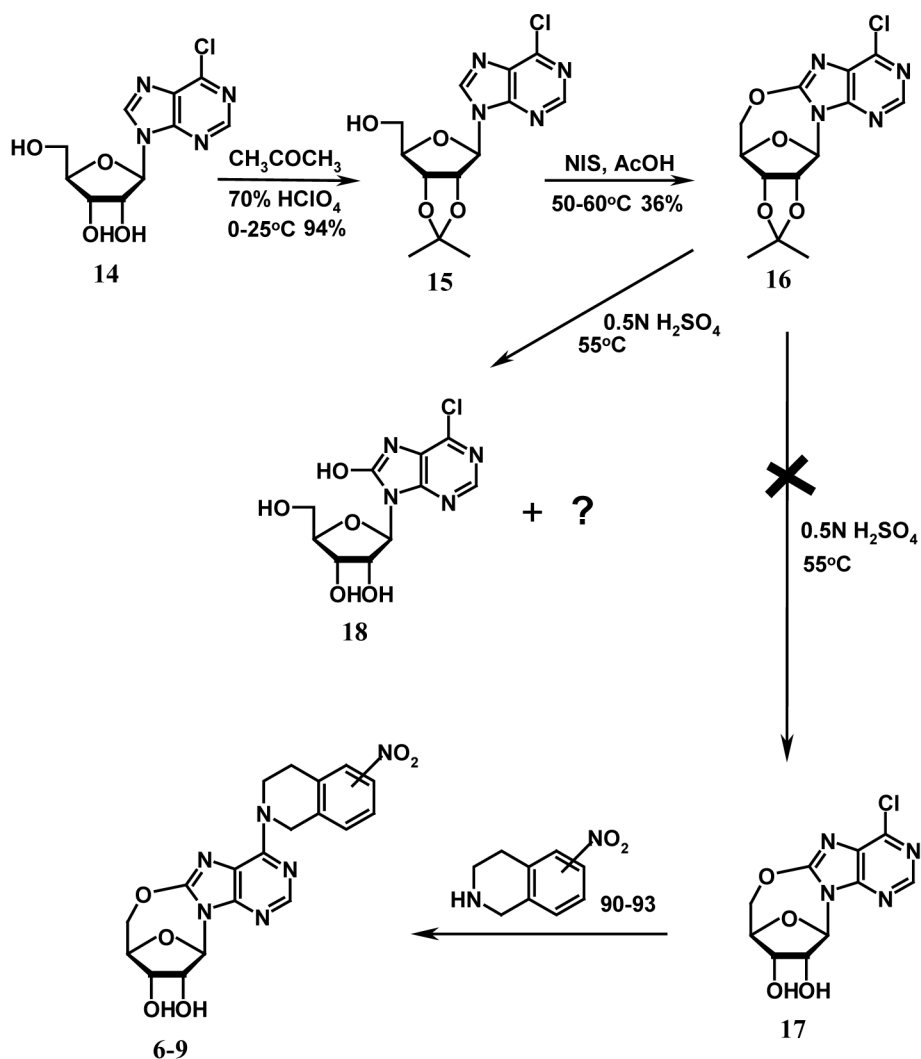
Figure 10. PLS coefficient*stdev steric and electrostatic contour maps of CoMFA 3D QSAR model. Red, negative electrostatic potential enhances potency; blue, positive electrostatic potential favors activity; green, bulky substituents enhance potency; yellow, bulky substituents are unfavorable to activity.



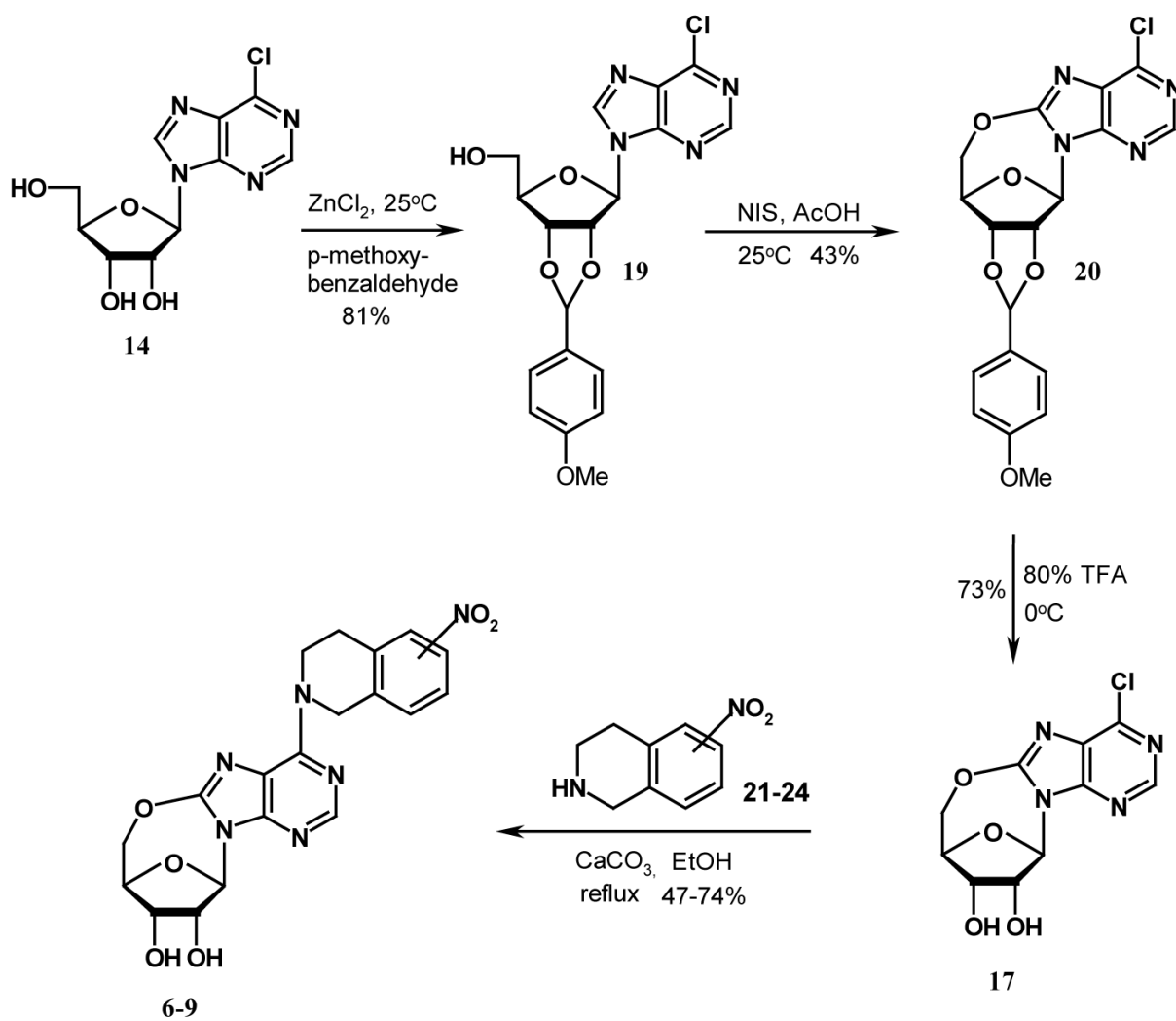
Scheme 1.



Scheme 2.



Scheme 3.

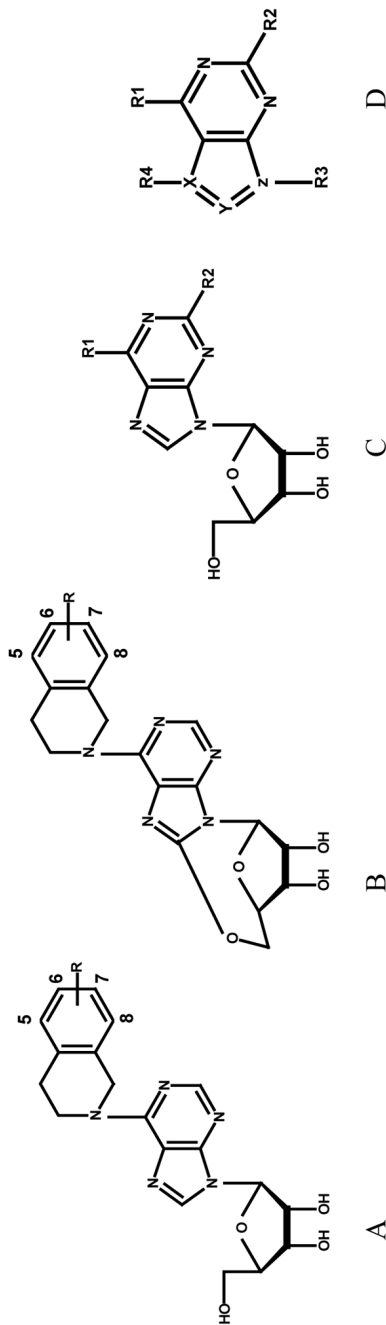


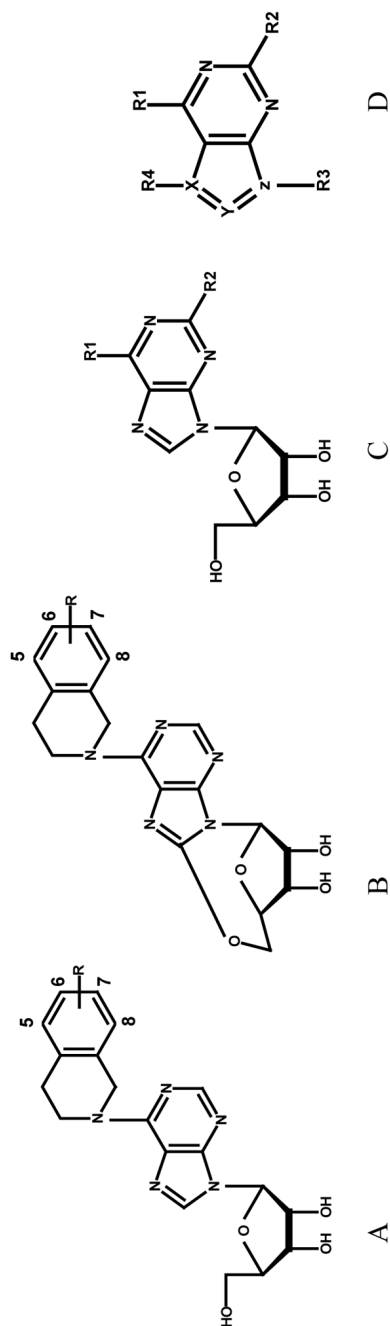
Scheme 4.

Table 1

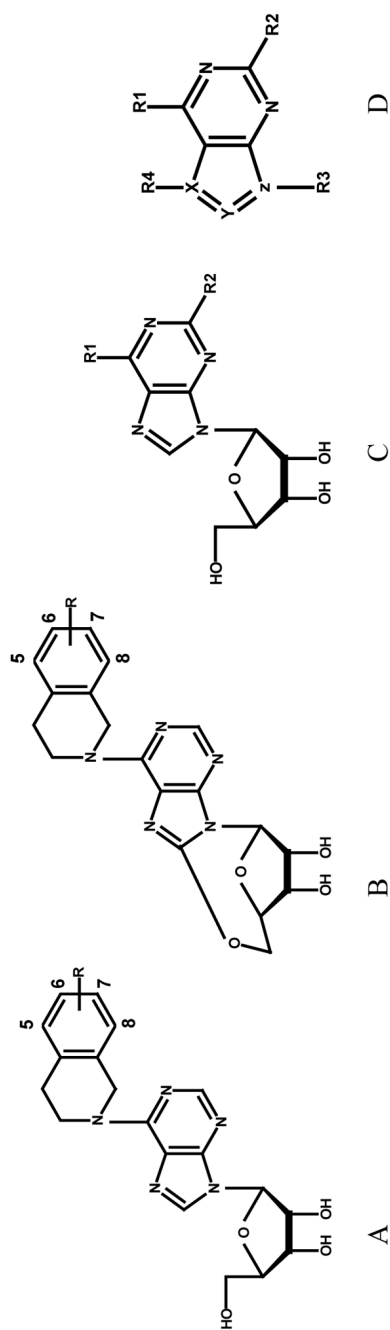
Structures and inhibitory activities of compounds in the training set.

Compd	Type	R	R ₁	R ₂	R ₃	R ₄	X	Y	Z	pIC ₅₀
1, NBMPR	C									8.07 ^d
2	A	5-NO ₂	-S ⁻ -(4-nitrobenzyl)	H						5.520 ^a
3	A	6-NO ₂								6.740 ^a
4	A	7-NO ₂								8.264 ^a
5	A	8-NO ₂								5.440 ^a
6	B	5-NO ₂								2.130 ^a
7	B	6-NO ₂								3.610 ^a
8	B	7-NO ₂								6.480 ^a
9	B	8-NO ₂								2.76 ^a
26	A	H								5.740 ^a
27	C			NH ₂						7.670 ^b
28	C			H						4.870 ^b
29	C			H						4.970 ^b
30	C			H						3.04 ^b
31	C			H						4.44 ^b
32	C			H						3.59 ^b
33	C			H						6.51 ^b
34	C			H						7.56 ^b
35	C			H						4.49 ^b
36	C			H						4.75 ^b
37	C			H						5.68 ^b
38	C			H						4.86 ^b
39	C			H						5.77 ^b
40	C			H						5.81 ^b
41	C			H						5.20 ^b
42	C			H						4.67 ^b
43	C			H						4.24 ^b
44	C			H						7.48 ^b





Compd	Type	R	R ₁	R ₂	R ₃	R ₄	X	Y	Z	pIC ₅₀
45	C		-S- (4-isopropylbenzyl)	H						5.32 ^b
46	C		-S- [(2-methyl-1-naphthyl)-methyl]	H						3.94 ^b
47	C		-S- methyl	H			N	C	N	3.64 ^b
48	D		-S- methyl	H	tetrahydropyran-2-yl					3.56 ^b
49	C		-S- phenylpropyl	H						5.87 ^b
50	C		-S- phenyl	H						4.04 ^b
51	C		-S- 2-methylbenzyl	H						5.20 ^b
52	C		-S- 3-methylbenzyl	H						4.92 ^b
53	C		-S- 4-methylbenzyl	H						6.34 ^b
54	C		-S- benzyl	NH ₂						5.28 ^b
55	C		-S- (3-bromo-benzyl)	NH ₂						5.54 ^b
56	C		-S- (4-bromo-benzyl)	NH ₂						6.09 ^b
57	D		-S- isopropyl	NH ₂	butyl		N	C	N	3.92 ^b
58	D		-S- methyl	NH ₂	butyl		N	C	N	3.66 ^b
59	D		-S- (2-pyridylmethyl)	NH ₂	butyl		N	C	N	4.28 ^b
60	C		-S- butyl	NH ₂						4.92 ^b
61	C		-S- sec-butyl	NH ₂						4.20 ^b
62	C		-S- (2-chloro-benzyl)	NH ₂						4.87 ^b
63	C		-S- ethyl	NH ₂						3.79 ^b
64	C		-S- (2-fluoro-benzyl)	NH ₂						5.32 ^b
65	C		-S- (4-fluoro-benzyl)	NH ₂						5.94 ^b
66	C		-S- (2-hydroxy-5-nitrobenzyl)	NH ₂						8.56 ^b
67	C		-S- iodo	NH ₂						4.09 ^b
68	D		-S- propyl	NH ₂	isobutyl		N	C	N	4.2 ^b
69	C		-S- isobutyl	NH ₂						5.06 ^b
70	D		-S- isopropyl	NH ₂	propyl		N	C	N	3.84 ^b
71	C		-S- isopropyl	NH ₂						3.72 ^b
72	D		-S- (2-pyridylmethyl)	NH ₂	2-methylbutyl		N	C	N	4.38 ^b
73	C		-S- (1-methyl-4-nitroimidazol-5-yl)	NH ₂						3.24 ^b
74	C		-S- (6-methyl-2-pyridylmethyl)	NH ₂						1.94 ^b
75	C		-S- methyl	NH ₂						3.69 ^b



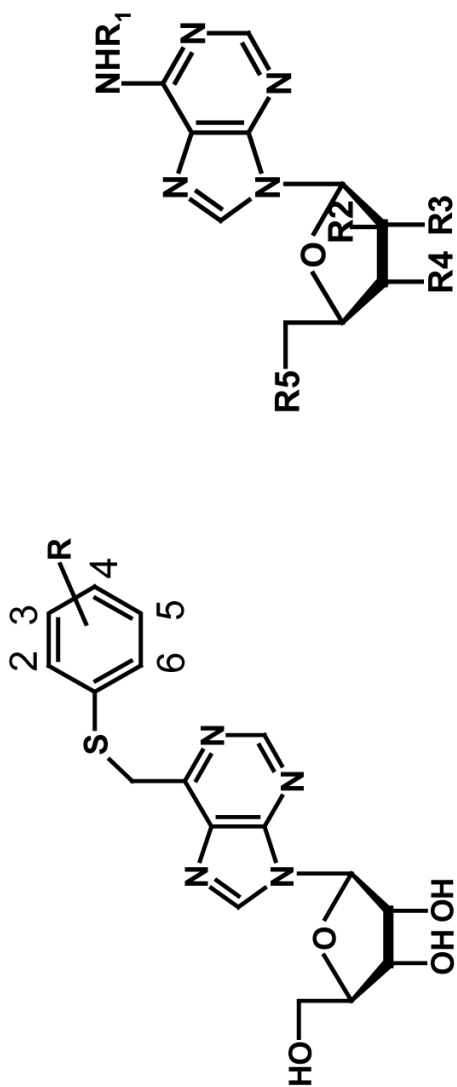
Compd	Type	R	R ₁	R ₂	R ₃	R ₄	X	Y	Z	pIC ₅₀
76	C		-S- 2-nitrobenzyl	NH ₂						5.34 ^b
77	C		-S- 3-nitrobenzyl	NH ₂						6.75 ^b
78	C		-S- phenethyl	NH ₂						4.79 ^b
79	D		-S- (2-pyridylmethyl)	NH ₂	propyl		N	C	N	4.04 ^b
80	C		-S- propyl	NH ₂						4.49 ^b
81	C		-S- (2-pyridyl-methyl)	NH ₂						4.46 ^b
82	C		-S- (3-pyridyl-methyl)	NH ₂						4.83 ^b
83	C		-S- (2-acetophenone)	NH ₂						3.35 ^b
84	C		-S- (4'-chloro-2-acetophenone)	NH ₂						4.84 ^b
85	D		-NH- isopentyl	H	H	H	C	N	N	3.63 ^b
86	D		-NH- phenethyl	H	H	H	C	N	N	4.00 ^b
87	D		-NH ₂	H	H	I	C	C	N	3.64 ^b
88	D		-S- benzyl	H	-β-D-ribofuranosyl	H	C	C	N	5.28 ^b
89	D		-S- methyl	H	-β-D-ribofuranosyl	Br	C	C	N	3.94 ^b
90	D		-chloro	H	-β-D-ribofuranosyl	I	C	C	N	4.11 ^b
91	D		-methoxy	H	-β-D-ribofuranosyl	H	C	C	N	3.47 ^b
92	D		-piperidino	H	-β-D-ribofuranosyl	H	C	C	N	3.71 ^b
93	D		-SH	H	-β-D-ribofuranosyl	H	C	C	N	3.41 ^b

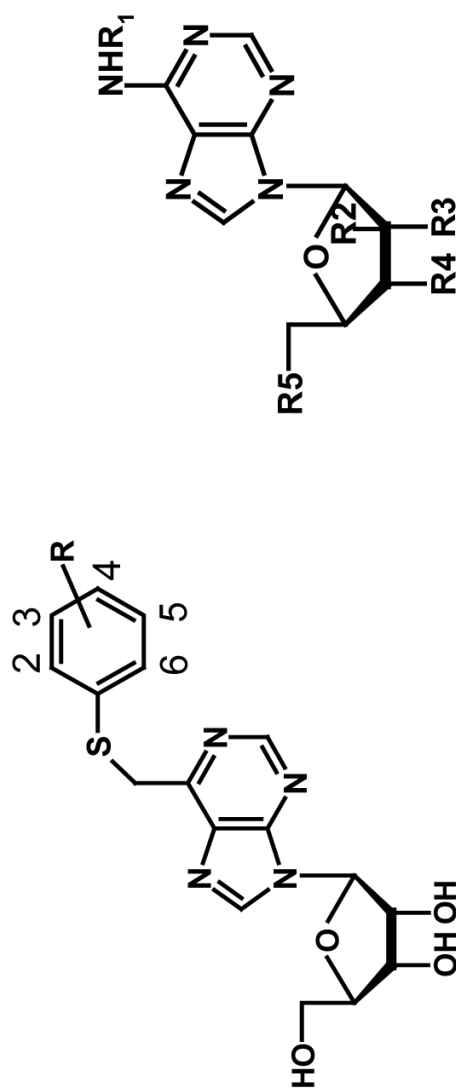
^aResults taken from Zhu *et al.*¹^bResults taken from Paul *et al.*²⁸

Table 2

Structures and inhibitory activities of compounds in the test set.

Compd	Type	R	R ₁	R ₂	R ₃	R ₄	R ₅	pIC ₅₀
94	A	2,4,6-trimethyl						4.48 ^b
95	A	2,4-dichloro						7.11 ^b
96	A	2-Br						5.62 ^a
97	A	2-Cl+6-F						5.82 ^b
98	A	2-Cl						5.75 ^a
99	A	2-F						6.45 ^a
100	A	2-I						6.55 ^a
101	A	3,4-dichloro						6.65 ^b
102	A	3-Br						6.44 ^a
103	A	3-CF ₃						6.48 ^b
104	A	3-Cl						6.55 ^a
105	A	3-F						6.70 ^a
106	A	3-I						6.61 ^a
107	A	3-NO ₂						8.32 ^b
108	A	4-Br						6.75 ^a
109	A	4-CN						7.09 ^b
110	A	4-COOCH ₃						6.09 ^b
111	A	4-Cl						6.60 ^a
112	A	4-F						6.80 ^a
113	A	4-I						7.16 ^a
114	A	4-OCF ₃						6.91 ^b





A

B

Compd	Type	R	R ₁	R ₂	R ₃	R ₄	R ₅	pIC ₅₀
115	A	4-OCH ₃						6.21 ^b
116	A	4-t-butyl						3.48 ^b
117	B		4-nitrobenzyl	OH	H	OH	OH	7.50 ^c
118	B		2-CH ₃ -3-NO ₂ benzyl	H	OH	OH	OH	6.37 ^c
119	B		2-Cl-4-NO ₂ benzyl	H	H	OH	OH	6.46 ^c
120	B		4-NO ₂ benzyl	H	H	OH	OH	7.80 ^c
121	B		2-NO ₂ -4-Cl benzyl	H	OH	OH	OH	4.33 ^c
122	B		2-NO ₂ -5-CH ₃ benzyl	H	OH	OH	OH	5.89 ^c
123	B		3-CH ₃ -4-NO ₂ benzyl	H	OH	OH	OH	7.06 ^c
124	B		4-NO ₂ benzyl	H	OH	H	OH	6.01 ^c
125	B		3-NO ₂ -4-CH ₃ benzyl	H	OH	OH	OH	5.93 ^c
126	B		3-NO ₂ -4-Cl benzyl	H	OH	OH	OH	6.15 ^c
127	B		3-OCH ₃ benzyl	H	H	OH	OH	3.94 ^c
128	B		4-acetamido benzyl	H	OH	OH	OH	6.74 ^c
129	B		4-Cl acetamido benzyl	H	OH	OH	OH	6.23 ^c
130	B		4-NH ₂ benzyl	H	OH	OH	OH	5.38 ^c
131	B		4-NO ₂ benzyl	H	H	OH	Cl	6.97 ^c
132	B		4-NO ₂ benzyl	H	OH	OH	H	7.66 ^c

^aResults taken from the literature.³⁰^bResults taken from the literature.³¹

^cResults taken from the literature.²⁹

Table 3Flow cytometrically-determined K_i values of 5'-O, 8-cyclo compounds.

5'-O, 8-cyclo series	K_i (nM)
6	> 1000
7	> 1000
8	18.89
9	> 1000
NBMPR ^a	0.70

^a NBMPR was added as a standard.

Table 4Comparison of the K_i values of the two series of conformationally constrained analogues of NBMPR^a.

Compound with a free glycosidic bond	K_i (nM)		K_i (nM)	5'-O-8-Cyclo compound
2	250	←	>1000	6
3	15	←	>1000	7
4	0.45	←	18.89	8
5	300	←	>1000	9

^aTwo-way arrows are showing corresponding K_i values

Table 5

The top five ranking pharmacophore hypotheses generated using PHASE.^a

Pharmacophore	Pharm_A	Pharm_B	Pharm_C	Pharm_D	Pharm_E
Ranking Features Conformation of aligned molecules	1 AAAHRR <i>anti</i>	2 AAAHRR <i>anti</i>	3 AADHRR <i>anti</i>	4 AAAHRRR <i>anti</i>	5 AADHRR <i>anti</i>

^aThe features defined in PHASE include: hydrogen bond acceptor (A), hydrogen bond donor (D), hydrophobic group (H), negatively charged group (N), positively charged group (P), and aromatic ring (R).

Table 6

PLS statistics of PHASE 3D QSAR models and prediction of test set.

Pharmacophore	Pharm_A	Pharm_B	Pharm_C	Pharm_D	Pharm_E
PLS Statistics of QSAR model					
r^2	0.916	0.886	0.901	0.923	0.929
<i>SD</i>	0.405	0.472	0.437	0.388	0.372
<i>F</i>	193.956	137.93	164.534	213.297	233.308
<i>P</i>	2.034e-37	1.081e-32	2.022e-35	9.200e-39	4.852e-40
PLS Components Results of test set					
Predictive r^2 for the external test set	0.777	-0.006	0.125	-0.184	-0.742

Table 7

PLS statistics of CoMFA 3D QSAR model.

PLS Statistics	CoMFA
q^2	0.591
r^2	0.894
s	0.472
F	188.072
PLS Components	5
Contribution	
steric	0.373
electrostatic	0.627

Table 8

Results of group cross-validation and randomization exercise for the CoMFA 3D-QSAR model.

Exercise	PLS Statistics	CoMFA
Group validation (20 runs)	Average q^2 (STDEV)	0.572 (0.032)
Randomization (20 runs)	Rand q^2	0.0005

Table 9

Residuals of the predictions of the test set by the CoMFA 3D QSAR model.

Compd	Actual pIC ₅₀	Residual	Compd	Actual pIC ₅₀	Residual
94	4.48	-0.9	114	6.91	0.93
95	7.11	0.67	115	6.21	0.25
96	5.62	0.02	116	3.480	-1.41
97	5.82	0.14	117	7.50	0.04
98	5.75	0.01	118	6.37	0.68
99	6.45	0.75	119	6.46	-0.29
100	6.55	0.77	120	7.80	-0.12
101	6.65	-0.34	121	4.33	-0.51
102	6.44	0.22	122	5.89	0.97
103	6.48	0.06	123	7.06	0.04
104	6.55	-0.01	124	6.01	0.13
105	6.70	0.36	125	5.93	0.17
106	6.61	0.53	126	6.15	-0.38
107	8.32	0.29	127	3.94	-0.25
108	6.75	0.36	128	6.74	0.89
109	7.09	-0.17	129	6.23	0.02
110	6.09	-0.77	130	5.38	0.49
111	6.60	0.03	131	6.97	0.12
112	6.80	0.3	132	7.66	0.27
113	7.16	0.91			